Eur. J. Mech. B/Fluids 18 (1999) 793–822
© 1999 Éditions scientifiques et médicales Elsevier SAS. All rights reserved

Mixing in Stokes flow in an annular wedge cavity

T.S. Krasnopolskaya [1], V.V. Meleshko [2], G.W.M. Peters, H.E.H. Meijer

Section of Materials Technology, Department of Mechanical Engineering, Eindhoven University of Technology, P.O. Box 513, 5600 MB Eindhoven, The Netherlands

(Received 3 March 1998; revised 20 February 1999; accepted 7 March 1999)

Abstract – The paper addresses a new approach for investigating and evaluating the basic properties of distributive laminar mixing in two-dimensional creeping flows by analysing a periodic Stokes flow in an annular wedge cavity. Flow is induced by the repetitive motion of the curved top and bottom walls, with prescribed velocities. An analytical solution for the velocity field in the cavity is presented, along with the algorithm for line tracking, which conserves the topological properties of any closed contour. A technique for finding all periodic points in the flow, and quantitative measures for the estimation of the mixing quality at any instant, are derived and applied to the flow in the wedge cavity. © 1999 Éditions scientifiques et médicales Elsevier SAS

Stokes flow / distributive laminar mixing / annular wedge cavity

1. Introduction

The purpose of this article is to examine the properties of distributive laminar mixing of highly viscous fluids by considering a two-dimensional Stokes flow in an annular wedge cavity. The flow is induced by a motion of the top and bottom curved walls with prescribed velocities, periodic in time, and can serve as a prototype for the flow between two neighbouring paddles of a periodically rotating turbine. Study of the mixing in the wedge cavity is special compared to other geometries because the annular wedge is the typical cross-section of a single screw extruder or a mixing element in any rotary device, which is always more realistic than, for example, a rectangular cavity. Analysis of the annular wedge cavity is a further step towards more realistic mixing configurations. We present the analytical solution for the velocity field in the cavity, the algorithm for line tracking of any contour enclosing some dyed region, the technique for finding the periodic points in the flow, and the quantitative measures for the estimation of the quality of mixing.

There is proposed a unique contour tracking algorithm that conserves both area and topological properties (connectedness and non-selfintersection) of any dyed blob and this provides an opportunity to calculate the length of blob's interface even under chaotic process. This cannot be done by the traditional technique of representing the blob's boundary as a collection of a great number of uniformly distributed material particles. The algorithm gives a new insight into properties of two-dimensional mixing under chaotic advection—the knowledge of the exact position of the whole blob inside the wedge cavity was exploited for the first time in modified statistical measures for quantifying the mixing quality and for gaining proper understanding of what is usually qualitatively estimated as a 'good' or a 'bad' mixture.

Mixing operations, as used in e.g. polymer, chemical and food processing, have been the subject of considerable study and research for several decades—see, for instance, review articles by Irving and Saxton [1],

[1] Correspondence and reprints; permanent address: Ukrainian Research Institute of the Environment and Resources, Kiev, Ukraine
[2] Permanent address: Institute of Hydromechanics, National Academy of Sciences, Kiev, Ukraine

Edwards [2], Ottino [3], and Ottino et al. [4], and separate chapters in the textbooks by Brodkey [5], Middleman [6], Ottino [7], Baird and Collias [8] for details. Despite these efforts, practical mixing has remained a more or less empirical art with little foundation in scientific analysis. Even a proper definition of the quality of mixing is not available yet and, in this paper, we address specifically this omission.

In contrast with that, a formal mathematical definition of mixing exists which was first introduced by Poincaré and developed in the mid-thirties by Birkhoff, von Neumann and Hopf (see, for example, Hopf [9], Aref [10] for a general discussion). This definition is (Arnold and Avez [11]) as follows: the process is called the mixing process, if for any given non-intersecting regions A and B at the initial moment, with measures $\mu(A)$ and $\mu(B)$, respectively, in a space V with measure $\mu(V)$ the measure $\mu(A \cap B)$ of the image of the region A, which is contained in the region B, after a sufficiently long time will tend to the value $\mu(A)\,\mu(B)/\mu(V)$.

An important feature of mixing systems is that the motion of an individual point is unstable. This means that two points, initially close together, deviate widely as time passes. Already Maxwell [12] and later Borel [13], Krylov [14,15] anticipated that the existence of unstable conditions, i.e. exponential divergence of trajectories of neighbouring points, implies the impossibility of predicting future events, if knowledge of the initial conditions is only approximate. Lighthill [16] introduced the notion 'horizon of predictability' as a characteristic feature of non-linear dynamical systems. Properties of such 'anomalous diffusion' of diverging neighbouring points have been studying in detail in theory of dynamical systems (Artuso [17]).

Spencer and Wiley [18] have defined that distributive laminar mixing of nonsoluble fluids can be thought of as consisting of two processes: increasing the interfacial surface between the fluids being mixed, and distributing that interface throughout the volume of material. The increase in interfacial surface leads to a decrease in the average striation thickness in the system. The mixing process is usually continued until the thickness of the striations becomes sufficiently small with respect to the scale on which the mixture is to be evaluated. Intuitively, good mixing requires that any dyed blob must be distributed so that in any chosen volume element the ratio of the components is the same as in the entire cavity.

The study of distributive mixing is based on a description of paths of a dyed blob individual particles. The use of the word 'particle' in this context is convenient, but requires some explanation. What is really investigated is the motion of a mathematical point that moves at each instant with the velocity corresponding to its instant position. Thus, the dyed particle is supposed to be inertialess, it is not subjected to diffusion, and no interfacial tension is operative. Although the idea of such an approach, connecting the Eulerian and Lagrangian representations of fluid flow, was laid down already by Maxwell [19] and developed later by Riecke [20], Morton [21] up to the recent time comparatively little has been done to apply these concepts in the analysis of mixing flows. The study of chaotic advection using of the Lagrangian description was pionereed by Aref [22]. An experimental paper by Chaiken et al. [23] have considered the streamline switching mechanism for generation of chaos in two-dimensional Stokes flow between eccentric cylinders. The whole issue was discussed in Aref and El Naschie [24].

The purpose of mixing is to achieve a uniform distribution of the components. The main practical question is, however, not whether the system will eventually approach this uniform distribution, but rather how much, at any moment in time, the mixing state deviates from a uniform state. Gibbs [25, Ch. 12], while considering ensembles in phase space going to statistical equilibrium (by the process which he called 'stirring'), suggested an analogy for this process in terms of the mixing of a coloured fluid in water. Assuming conservation of the amount of coloured liquid which does not affect hydrodynamic properties of flow, incompressibility and mutual insolubility of both liquids, one can realize that the 'colour' density (of value 0 or 1) at any point will remain unchanged, as does the mean square density (which one might expect to provide a measure of the deviation from completely uniform mixing). On the other hand, if one fixes the size of the spatial elements (boxes), defines the density inside the every box and continues the mixing indefinitely long, then the mean

square density does decrease to a minimum. In order to sharpen this distinction, the Ehrenfests [26] introduced the terms ‘fine-grained density’ and ‘coarse-grained density’ for these two conceptions.

The traditional approach, based upon the presentation of the dyed blob as a collection of N points uniformly distributed over the area S_b of the blob, can provide a reasonable treatment of mixing with excellent correspondence with the experiments, even in complex domains (Jana et al. [27]). For long time evolutions, however, this approach provides only a qualitative general picture of mixing (see Liu et al. [28] for several examples). Fine details, especially the question whether an ‘empty’ space surrounded by a cluster of points really means the absence of the component to be mixed, remain unclear. Basically, the uniformly distributed multipoint approach can not provide a valid description of blob stretching and folding, if the thickness of filaments becomes less than $(S_b/N)^{1/2}$, or if the length of the contour line becomes more than $2(NS_b)^{1/2}$. Besides, being distributed uniformly at the initial moment, the points tend to spread out nonuniformly and, sometimes, collect into dense clusters. Any ‘box-counting’ calculations based upon the preservation of a Lebesgue measure of the set of N points (with an ‘area’ S_b/N associated with each point), can provide only qualitative estimates for quality of mixing.

The problem of mechanical mixing, which we deal with in this paper, differs essentially from the mathematical mixing systems. We restrict our consideration to finite times and are mainly interested in how to organize steady or periodic flows and where to put the blob (or blobs) in order to achieve the best result in that finite time.

Figure 1 demonstrates flow patterns for a two-dimensional steady motion in an annular wedge cavity while moving either the bottom or top wall. Obviously, they are not the examples of good mixing—the mixing domain (light-green colour) is limited here by closed steady streamlines and does not spread over the whole cavity.

Figure 2 shows three typical pictures of a mixture in the annular wedge cavity after ten periods of periodic motion of the bottom and top walls, with the same total wall displacement as for the steady motion. Comparison of *figures 1* and *2* shows that, despite of the same ‘energy-input’, the results of mixing are completely different.

Our analysis of distributive mixing is based upon a conservation of topological properties (connectedness and orientation) of the Lagrangian interface line between components deformed by an Eulerian velocity field. The key idea of our approach is the use of a non-uniform distribution of points at the initial contour to represent this interface, such that (i) the distance between neighbouring points remains between some chosen values (that is, points are added when the distance becomes too long and points are removed when it becomes too short) and (ii) the angle between any neighbouring straight lines is greater than some prescribed value (to describe folding of the line). The principal advantage of this approach for line tracking is that area preservation of the blob enclosed by the contour is guaranteed, even after complicated stretching and folding. Knowing the position of the contour line, we can construct an Eulerian description of the deformation process, giving an opportunity to quantify mixing at any moment of time.

When the motion of the walls is periodic in time, the Stokes flow velocity field inside the cavity is also periodic. The study of particle motions in a periodically driven velocity field can be reduced to the study of a discrete time system by means of Poincaré mapping—series of positions of points taken stroboscopically at each period. This reduces the analysis of dynamical systems to problems that could be stated more simply, yet retain their essential ingredients. Fixed points of such a mapping correspond to the closed periodic trajectories of the particle under consideration that are closed after one, two, or more full periods. Therefore, it is important to find the positions of these periodic points in the flow and to discover whether they are numerous or relatively few. Given some spatial symmetry of the velocity field in the cavity we apply, similar to Meleshko and Peters [29], the symmetry arguments. They were first suggested by de Vogelaere [30] and developed by Franjione et al. [31] and Franjione and Ottino [32]. Apart from the position, each periodic point must also be classified (as elliptic, parabolic or hyperbolic) by using linearized mapping in its immediate vicinity.

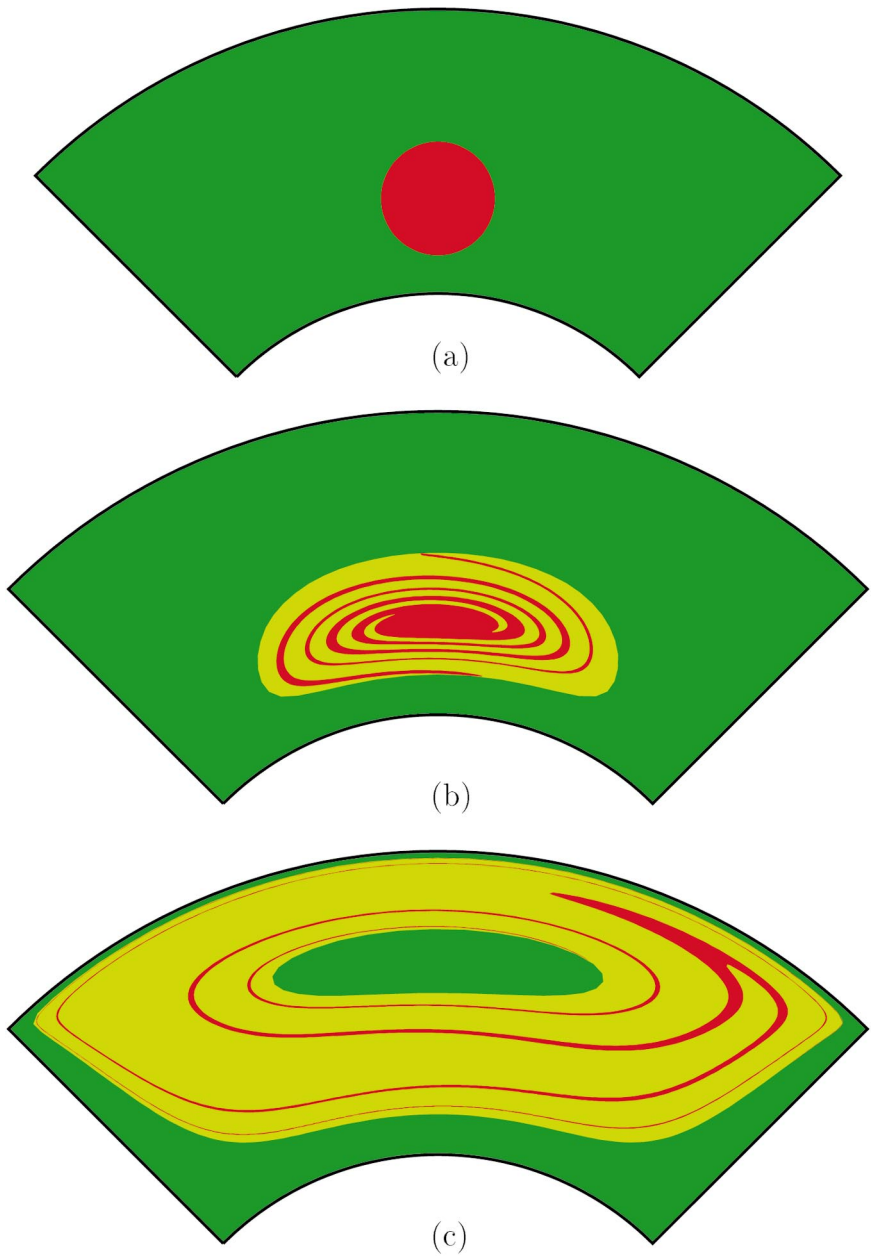

Figure 1. Mixing patterns: (a) initial position of a circular blob and the blob under steady motion of (b) the bottom wall; (c) the top wall.

Knowledge about the location and type of periodic points allows us to determine optimal mixing regimes, and yields opportunities to identify coherent structures in the mixing patterns (Meleshko et al. [33]).

We will adopt Gibbs' approach and use the 'coarse-grained density' of the distribution as a basic measure for the three criteria of the mixed state: the mean square density (Welander [34]), the entropy (Gibbs [25]) and the intensity of segregation (Danckwerts [35]). All three criteria show the dynamics of mixing in their own scales and may be used descriptively but never causatively, which was explained by Ben-Naim [36]. By using these criteria we can for a given volume element size (the 'grain') estimate the time necessary for the mixed state

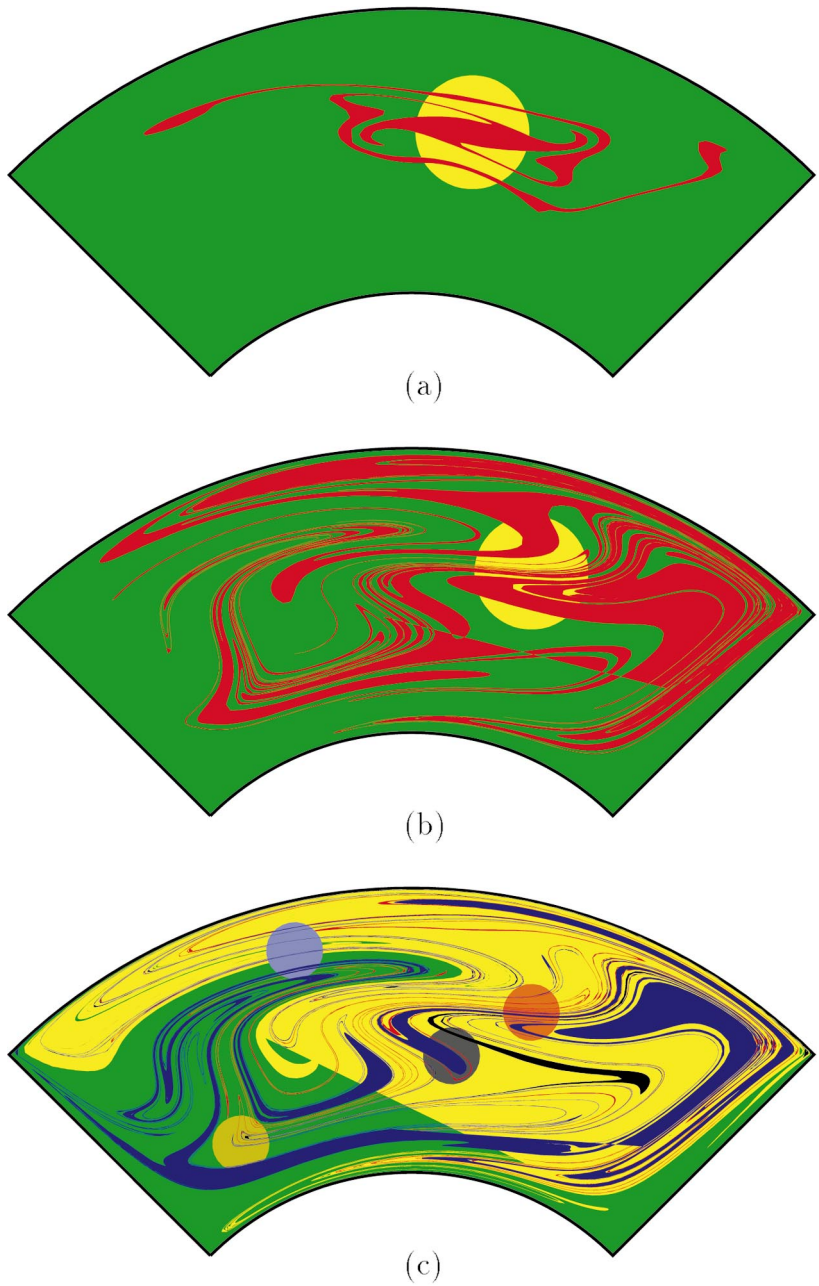

Figure 2. Mixing patterns obtained for the same input energy, by adjusting the initial position of the circular blob (a) surrounding an elliptic point; (b) hyperbolic point; (c) divided into four different small blobs.

to be uniform within some specified range. The larger the element size, the faster this desired mixed state is reached. The three criteria are not independent, and they are statistical measures of the first order (Tucker [37]). For a more complete description of a mixture, we will also use the scale of segregation (Danckwerts [35]) which is a statistical measure of the second order. It represents an average of the size of the clumps of the mixed component.

The paper is organized as follows: The problem of mixing in the annular wedge cavity is stated in Section 2, combined with an analytical expression for the velocity field in the cavity as well as numerical algorithms for contour line tracking, searching for and classifying periodic points and the main definitions of measures for the quality of mixing. In Section 3 the results of numerical studies of mixing with various protocols of wall movement are given and discussed. Finally, some conclusions are outlined in Section 4.

2. Theory and methods

2.1. Problem statement

We consider a two-dimensional creeping flow of incompressible viscous fluid in an annular wedge cavity, $a \leqslant r \leqslant b,\ |\theta| \leqslant \theta_0$ (*figure 3*), caused by tangential periodically time-dependent velocities V_{bot} and V_{top} at the curved bottom and top boundaries $r = a$ and $r = b$, respectively. The side walls, $a \leqslant r \leqslant b,\ |\theta| = \theta_0$ are fixed. We restrict our consideration to the discontinuous mixing protocol when, during each half of the period $T/2$, the bottom or top wall rotates over an angle Θ clockwise and counterclockwise, respectively:

$$\begin{cases} V_{\text{bot}}(t) = \dfrac{2a\Theta}{T}, \quad V_{\text{top}}(t) = 0, & \text{if } kT < t \leqslant \left(k + \dfrac{1}{2}\right)T, \\ V_{\text{bot}}(t) = 0, \quad V_{\text{top}}(t) = -\dfrac{2b\Theta}{T}, & \text{if } \left(k + \dfrac{1}{2}\right)T < t \leqslant (k+1)T. \end{cases} \tag{1}$$

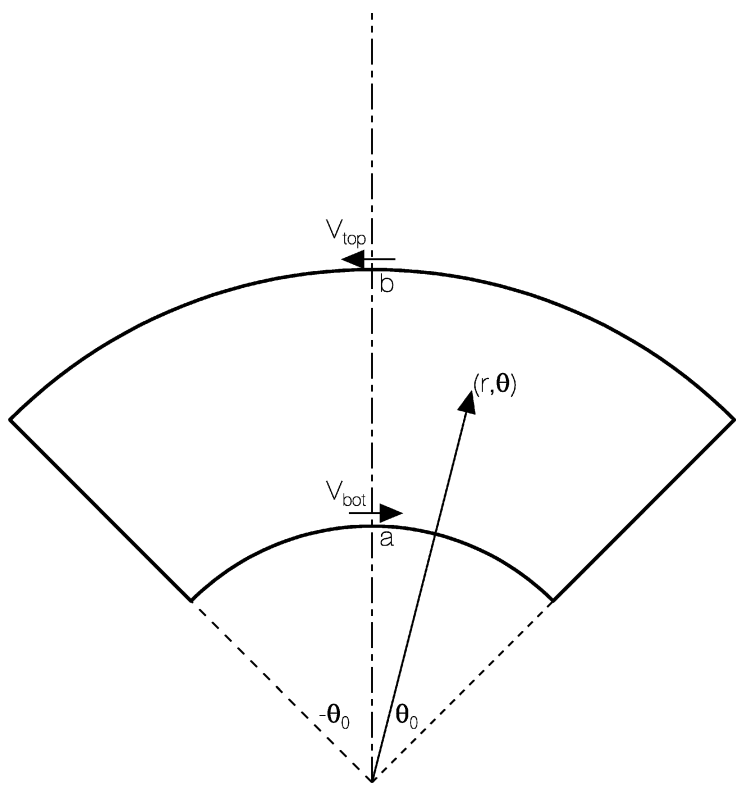

Figure 3. Geometry of the annular wedge cavity.

The radial u_r and azimuthal u_θ components of velocity can be expressed by means of the stream function Ψ as

$$u_r = \frac{1}{r}\frac{\partial \Psi}{\partial \theta}, \qquad u_\theta = -\frac{\partial \Psi}{\partial r}. \tag{2}$$

For the Stokes flow approximation the stream function Ψ satisfies the biharmonic equation

$$\nabla^2 \nabla^2 \Psi = 0 \tag{3}$$

(∇^2 stands for the Laplace operator) with the boundary conditions

$$\begin{cases} \Psi = 0, & \dfrac{\partial \Psi}{\partial r} = -V_{\text{bot}}, & \text{at } r = a,\ |\theta| \leqslant \theta_0, \\ \Psi = 0, & \dfrac{\partial \Psi}{\partial r} = -V_{\text{top}}, & \text{at } r = b,\ |\theta| \leqslant \theta_0, \\ \Psi = 0, & \dfrac{\partial \Psi}{\partial \theta} = 0, & \text{at } a \leqslant r \leqslant b,\ |\theta| = \theta_0. \end{cases} \tag{4}$$

Therefore, we have the classical biharmonic problem for the stream function Ψ with prescribed values of the function and its outward normal derivative at the boundary.

The system of ordinary differential equations

$$\frac{dr}{dt} = \frac{1}{r}\frac{\partial \Psi}{\partial \theta}, \qquad \frac{d\theta}{dt} = -\frac{\partial \Psi}{\partial r} \tag{5}$$

with the initial conditions $r = r_{\text{in}},\ \theta = \theta_{\text{in}}$ at $t = 0$ describes the motion of a passively advected individual (Lagrangian) particle which occupies the position (r, θ) at time t in the known Eulerian velocity field.

System (5) can be written in a Hamiltonian form. Besides the obvious transformation to the rectangular coordinates $x = r\sin\theta,\ y = r\cos\theta$, by which system (5) can be written in a traditional appearance

$$\frac{dx}{dt} = \frac{\partial \Psi_c}{\partial y}, \quad \frac{dy}{dt} = -\frac{\partial \Psi_c}{\partial x}, \quad \Psi_c(x, y, t) \equiv \Psi\left(\left(x^2 + y^2\right)^{1/2}, \arctan\frac{x}{y}, t\right), \tag{6}$$

it can be directly transformed into

$$\frac{d(r^2)}{dt} = \frac{\partial \widetilde{\Psi}}{\partial \theta}, \quad \frac{d\theta}{dt} = -\frac{\partial \widetilde{\Psi}}{\partial (r^2)}, \quad \widetilde{\Psi}\left(r^2, \theta, t\right) \equiv 2\Psi\left(\left(r^2\right)^{1/2}, \theta, t\right), \tag{7}$$

with r^2 and θ being conjugate variables.

Within time intervals $(kT, kT + T/2),\ (kT + T/2, kT + T)$ $(k = 0, 1, 2, \ldots)$, when the stream function does not explicitly depend on time, system (5) is integrable and there exists the first integral $\Psi(r, \theta) = \text{constant}$. Consequently, particle $(r_{\text{in}}, \theta_{\text{in}})$ moves along a steady streamline during the first half-period $(0, T/2)$. At the instant $t = T/2$ the topology of streamlines is instantaneously changed, and the particle moves along a new streamline during the second half-period $(T/2, T)$, and so on. The spatial position of the particle is continuous, but its velocity experiences a discontinuity at each moment $t_k = kT/2$.

The problem of mixing of a certain amount of dyed matter (the blob) which does not affect the velocity field in the cavity, consists in tracking the positions of particles initially occupying the contour of the blob, say, the

circle of radius R with the centre at (r_c, θ_c). We assume that the flow provides only a continuous transformation of the initially simply connected blob. Therefore, the deformed contour of the blob gives the whole picture of the mixing.

The question of how to track this closed contour in the periodically changing velocity field represents a separate numerical problem. The obvious solution of using a collection of initially equidistantly spaced points can cause problems after several periods. Therefore, an important part of our mixing analysis consists in the development of an effective numerical algorithm for contour tracking.

The problem of finding periodic points in the flow can be transformed into the problem of the two-dimensional search for the roots of some nonlinear equations. It is well known (Press et al. [38, p. 372]) that there are no good, general methods for finding the roots of nonlinear sets of algebraic equations. Here, the situation is even more complicated as the mapping of a point after each period is defined by a system of differential equations, and not an algebraic system. A two-dimensional search strategy for periodic points can take too much computing time. Consequently, we need to develop some numerical algorithm to find all such points, or at least those of lower order.

Finally, we need some quantitative measures for characterizing the quality of mixing in order to compare the results of various mixing protocols and those from varying the initial positions of the blob.

2.2. Methods used

In this section, the determination of the velocity field will be dealt with in Section 2.2.1. Accordingly, the problem of contour line tracking will be addressed in Section 2.2.2. Next, the periodic points are identified in Section 2.2.3. Finally, the definition of different mixing measures will be treated in Section 2.2.4.

2.2.1. The Eulerian velocity field in the cavity

To find the velocity field in the cavity, we apply the method of superposition to the boundary problem (3)−(4). The essence of that approach is provided by Krasnopolskaya et al. [39] and here we present only the main results.

The stream function in the wedge cavity can be written as

$$\begin{aligned}\Psi = {} & R_b\left(\frac{r^2}{a^2}-1\right)S\left(\frac{a}{r},\theta\right) - R_t\left(1-\frac{r^2}{b^2}\right)S\left(\frac{r}{b},\theta\right) \\ & + F_b r\, P_+(\rho,\theta) + F_t r\, P_-(\rho,\theta) + r\sum_{n=1}^{\infty}\frac{z_n}{\beta_n}P_n(\theta)\sin\beta_n\rho \\ & - \sum_{m=1}^{\infty}\frac{(-1)^m}{\alpha_m}\left\{\left(\frac{r^2}{a^2}-1\right)\left[(x_m+R_b)\,r_0^{\alpha_m}\left(\frac{r}{b}\right)^{\alpha_m} - x_m\left(\frac{a}{r}\right)^{\alpha_m}\right]\right. \\ & \left. + \left(1-\frac{r^2}{b^2}\right)\left[(y_m+R_t)\,r_0^{\alpha_m}\left(\frac{a}{r}\right)^{\alpha_m} - y_m\left(\frac{r}{b}\right)^{\alpha_m}\right]\right\}\cos\alpha_m\theta, \end{aligned} \tag{8}$$

with

$$\alpha_m = \left(m-\frac{1}{2}\right)\frac{\pi}{\theta_0}, \qquad \beta_n = \frac{n\pi}{l_0}, \qquad l_0 = \ln\frac{b}{a}, \qquad r_0 = \frac{a}{b}, \qquad \rho = \ln\frac{r}{a},$$

$$R_b = \frac{\pi^2\, a\, V_{\text{bot}}}{\theta_0\,(4-\pi^2)}, \qquad R_t = \frac{\pi^2\, b\, V_{\text{top}}}{\theta_0\,(4-\pi^2)}, \qquad F_b = \frac{4\pi\, a\, V_{\text{bot}}}{l_0\,(\pi^2-4)}, \qquad F_t = \frac{4\pi\, b\, V_{\text{top}}}{l_0\,(\pi^2-4)},$$

and

$$P_n(\theta) = \frac{\cosh \beta_n \theta}{\cosh \beta_n \theta_0} \cos\theta \, \sin\theta_0 - \frac{\sinh \beta_n \theta}{\sinh \beta_n \theta_0} \sin\theta \, \cos\theta_0. \tag{9}$$

The following notations

$$S(\xi, \theta) = \frac{\theta_0}{\pi} \arctan\left[\frac{2\xi^{\pi/2\theta_0} \cos(\pi\theta/2\theta_0)}{1 - \xi^{\pi/\theta_0}}\right], \tag{10}$$

$$P_+(\rho, \theta) = \sum_{n=1}^{\infty} \frac{1}{\beta_n} P_n(\theta) \sin \beta_n \rho, \qquad P_-(\rho, \theta) = \sum_{n=1}^{\infty} \frac{(-1)^n}{\beta_n} P_n(\theta) \sin \beta_n \rho \tag{11}$$

were introduced. The functions $P_+(\rho, \theta)$ and $P_-(\rho, \theta)$ can be transformed (see Appendix) into the fast convergent series.

The sets of coefficients x_m, y_m, and z_n are defined from the two fully regular infinite systems of linear algebraical equations, that can be effectively solved by simple reduction method. The knowledge of the asymptotic behaviour

$$x_m = \mathrm{O}\left(\alpha_m^{-\mathrm{Re}\,\gamma_1}\right), \quad y_m = \mathrm{O}\left(\alpha_m^{-\mathrm{Re}\,\gamma_1}\right), \quad m \to \infty, \qquad z_n = \mathrm{O}\left(\beta_n^{-\mathrm{Re}\,\gamma_1}\right), \quad n \to \infty \tag{12}$$

($\gamma_1 = 2.74 + i\,1.12$ is the root with the lowest positive real part of the equation $\sin(\pi\gamma/2) + \gamma = 0$) is important.

Because of the asymptotic behaviour (12), the infinite sums in (8) (along with their term by term first derivatives in r and θ) converge rapidly in the whole domain including the boundary. Therefore, it is sufficient to leave only a few first terms in these series (usually, up to five) when performing numerical calculations. Also, the first derivatives of the functions $S(a/r, \theta)$ and $S(r/b, \theta)$ provide a finite contribution to the velocity field at the boundary that can be calculated by taking the limits.

It is worth noting that the terms with R_b, R_t, F_b and F_t in expression (8) correspond locally to the Goodier [40] and Taylor [41] solution for Stokes flow in a quarter plane with a discontinuous tangential velocity applied along one side (see Batchelor [42, p. 224]). Such a local representation of the stream function near the corner points as well as the amplitude of the Moffatt [43] corner eddies is presented in Krasnopolskaya et al. [39].

Thus, the components of the velocity field can be calculated as the corresponding first derivatives of the stream function (8) in the form of rapidly converging series in the whole domain including the boundary. The numerical calculations of the velocity are fast and accurate.

2.2.2. Contour line tracking

Any algorithm of contour line tracking comes down to the tracking of points distributed along the initial blob boundary and, after this point tracking, connecting neighbouring points. Being obviously easy for the initial boundary, the general problem of how to connect these points by a smooth curve, without intersections in order to get the boundary at any instant, provides some difficulties. Because of nonuniform stretching and folding of the line, two neighbouring points may appear far away from each other at some future time. The obvious way to overcome this problem is to increase the number of points. In order to avoid much computational effort, this should not be done uniformly—but only at those parts of the initial line where considerable stretching or folding occurs. The essence of our algorithm is clear:

(i) Divide the time interval during which we want to analyze mixing into small time steps $\Delta t = 0.1T$. Start at $t_0 = 0$ with a small number of points N_0 (usually, $N_0 = 25$) uniformly distributed along the initial contour line. Solve system (5) for each point and trace the positions of all these points up to the moment $t_1 = \Delta t$.

(ii) Calculate the distance Δl_n between points of numbers n and $n+1$. If it appears that some distance Δl_k becomes larger than some initially prescribed value l_{dis} (usually, $l_{\text{dis}} = 0.02a$), insert an additional point on the initial contour in the middle between points k and $k+1$, solve the system (6) for that one point, and renumber correspondingly the initial and final arrays of points. After completing this operation we have $N_d \geqslant N_0$ points with distances between each of two neighbors less than l_{dis}. Connect these points by straight lines and form a N_d-polygon.

(iii) Take in any turn three points $m-1, m, m+1$ ($m = 2, 3, \ldots, N_d + 1$) and find the angle γ_m at the vertex m (computationally, it is preferable to calculate only the cosine of this angle from known distances between these points). If angle γ_m appears to be smaller than some prescribed value γ (usually, $\gamma = 120°$), insert additional points at the initial contour line between points $m-1, m, m+1$ in such a way that, finally, the distances between all 'old' and 'new' points do not exceed the value l_{cur} (usually, $l_{\text{cur}} = 0.005a$) or the angles in the polygon are larger than γ.

Thus, starting at $t_0 = 0$ with N_0 points uniformly distributed along the blob boundary, at the instant $t_1 = \Delta t$ we have N_1 points (with $N_1 \geqslant N_0$) that can be connected by straight lines to form a N_1-polygon. This polygon represents the deformed boundary at the moment t_1 and has the properties that distance between any two adjoint vertexes is smaller than l_{dis} (or, sometimes, l_{cur}) and that the angle at any vertex is not less than γ. It is important that this polygon has a direct correspondence to the nonuniform distribution of N_1 points on the initial line. The next step is now obvious: proceeding to the instant $t_2 = 2\Delta t$ we move firstly the N_1-vertex polygon and then apply the same algorithm again.

The proposed algorithm has the main advantage that all final points have their starting positions on the original contour. This aspect is usually lost when spline techniques are used to smooth the line and redistribute the points.

Numerical integration of system (6) within the time interval Δt was performed using two numerical ordinary differential equation integrators. The first of these is the standard explicit fourth-order Runge–Kutta method (Press et al. [38, Ch. 16]) with constant time step $0.005T$. The second is a Runge–Kutta–Fehlberg scheme with adaptive stepsize (Hairer et al. [44]).

An additional and important check of the proposed algorithm is the accuracy of fulfilling the area conservation condition. The area inclosed by the deformed curve was calculated via the Stokes theorem as a line integral, using the trapezoidal rule. The relative error was less than 0.1% for cases tested.

2.2.3. Periodic points and invariant manifolds

The proposed algorithm of search for periodic points reduces the two-dimensional search over the whole cavity to a one-dimensional search procedure of specific values r^* along the central line $\theta = 0$.

Consider a point $(r_{T/4}, 0)$ which at instant $t = T/4$ is located on the line of symmetry $\theta = 0$. Because of the symmetry of protocol (1) in time, it is obvious that at instant $t = 0$ and $t = T/2$ this point occupies the positions $(r_1, -\theta_1)$ and (r_1, θ_1), respectively. Now, if at instant $t = 3T/4$ this point is again on the line of symmetry $\theta = 0$ with coordinates $(r_{3T/4}, 0)$, then at the instants $t = T/2$ and $t = T$ its positions are (r_1, θ_1) and $(r_1, -\theta_1)$, respectively. Therefore, the point $(r_1, -\theta_1)$ is a periodic point of period 1, and the scenario $[T/4 - 3T/4]$ can be written as following:

– take at $t = T/4$ any point $(r_{T/4}, 0)$ on the symmetry line, integrate the advection system (5) up to $t = 3T/4$, and check whether the point $(r_{3T/4}, \theta_{3T/4})$ is located on the symmetry line. Thus, if r^* is the root of equation

$$\theta_{(T/4,3T/4)}(r^*, 0) = 0 \tag{13}$$

(here and in what follows, the indexes in circular brackets show the interval within which system (5) is integrated and the arguments represent the initial conditions for that system), then the point $(r_1, -\theta_1)$ with $r_1 = r_{(T/4,T/2)}(r^*, 0),\ \theta_1 = \theta_{(T/4,T/2)}(r^*, 0)$ is a periodic point of period 1.

Geometrically, this periodic point is located at the intersection of two steady streamlines $\Psi_{\text{bot}}(r, \theta) = C_{\text{bot}}$ and $\Psi_{\text{top}}(r, \theta) = C_{\text{top}}$, corresponding to the motion of the bottom and top wall, respectively. Only along these two paths can the periodic point return to its original position.

The type of a periodic point (elliptic or hyperbolic) can be classified analytically, by looking for the eigenvalues λ_1 and λ_2 of the Jacobian matrix $\mathbf{M}$ of the linearized mapping at this point. The elements of the Jacobian matrix $\mathbf{M}$ are calculated numerically by solving system (6) written in rectangular coordinates for the four initial conditions $(\bar{x} + \varepsilon, \bar{y}),\ (\bar{x} - \varepsilon, \bar{y}),\ (\bar{x}, \bar{y} + \varepsilon),\ (\bar{x}, \bar{y} - \varepsilon)$ (here $(\bar{x}, \bar{y})$ are the rectangular coordinates of the periodic point) and for small ε (usually, $\varepsilon = 0.005a$)

$$\begin{cases} M_{xx} = \dfrac{x_{(0,T)}(\bar{x} + \varepsilon, \bar{y}) - x_{(0,T)}(\bar{x} - \varepsilon, \bar{y})}{2\varepsilon}, & M_{xy} = \dfrac{x_{(0,T)}(\bar{x}, \bar{y} + \varepsilon) - x_{(0,T)}(\bar{x}, \bar{y} - \varepsilon)}{2\varepsilon}, \\ M_{yx} = \dfrac{y_{(0,T)}(\bar{x} + \varepsilon, \bar{y}) - y_{(0,T)}(\bar{x} - \varepsilon, \bar{y})}{2\varepsilon}, & M_{yy} = \dfrac{y_{(0,T)}(\bar{x}, \bar{y} + \varepsilon) - y_{(0,T)}(\bar{x}, \bar{y} - \varepsilon)}{2\varepsilon}. \end{cases} \tag{14}$$

The condition that the determinant of matrix $\mathbf{M}$ must be equal to unity is used to check the accuracy of calculations. If λ_1 and λ_2 are complex conjugates, the periodic point is elliptic. If λ_1 and $\lambda_2 = 1/\lambda_1$ are real, the periodic point is hyperbolic. Also the situation $\lambda_1 = \lambda_2 = \pm 1$ can exist, but this corresponds to the degenerated case of a parabolic periodic point: any small change in the mixing protocol (i.e. the value of Θ) leads to a periodic point of the elliptic or hyperbolic type.

For a hyperbolic periodic point there exist two invariant curves named the stable and unstable manifolds. These manifolds can be constructed by surrounding a periodic hyperbolic point by a small circle of radius $0.001a$ and then using the above-mentioned algorithm of contour line tracking under forward and backward mixing protocol (1). The backward mapping can be obtained by changing in (1) Θ to $-\Theta$ and starting with the movement of the top wall.

For finding periodic points of higher periods the following algorithms can be developed:

Period 2:

– scenario $[T/4 - 5T/4]$: if r^{**} is the root of equation $\theta_{(T/4,5T/4)}(r^{**}, 0) = 0$, then point (r_2, θ_2) with $r_2 = r_{(T/4,T/2)}(r^{**}, 0),\ \theta_2 = -\theta_{(T/4,T/2)}(r^{**}, 0)$ is a periodic point.
– scenario $[3T/4 - 7T/4]$: if r^{**} is the root of equation $\theta_{(3T/4,7T/4)}(r^{**}, 0) = 0$, then point (r_2, θ_2) with $r_2 = r_{(3T/4,3T/2)}(r^{**}, 0),\ \theta_2 = -\theta_{(3T/4,3T/2)}(r^{**}, 0)$ is a periodic point.

Period 3:

– scenarios $[T/4 - 7T/4],\ [3T/4 - 9T/4],\ [5T/4 - 11T/4]$.

Period 4:

– scenarios $[T/4 - 9T/4],\ [3T/4 - 11T/4],\ [5T/4 - 13T/4],\ [7T/4 - 15T/4]$.

Period 5:

– scenarios $[T/4 - 11T/4],\ [3T/4 - 13T/4],\ [5T/4 - 15T/4],\ [7T/4 - 17T/4],\ [9T/4 - 19T/4]$.

Period 6:

– scenarios $[T/4 - 13T/4]$, $[3T/4 - 15T/4]$, $[5T/4 - 17T/4]$, $[7T/4 - 19T/4]$, $[9T/4 - 21T/4]$, $[11T/4 - 23T/4]$.

Every periodic point of period n has $n - 1$ satellites, corresponding to their positions at instants T, $2T, \ldots, (n-1)T$. Therefore, the scenarios do not always supply new periodic points—only some satellites of others. In any case, these algorithms provide an effective search procedure of periodic points in the annular wedge cavity.

2.2.4. Evaluation of mixture quality

In this subsection we present a methodology for the evaluation of the quality of distributive mixing based on the statistical quantities, such as coarse-grained values of density, entropy, scale of segregation and intensity of segregation.

By dividing the cavity area S into N_δ square boxes of a side size δ with an area $S_\delta = \delta^2$ each, the cavity area can be written as $S = N_\delta S_\delta$. The conservation of coloured material area enclosed by the contour line permits us to introduce a probability function for the dyed material distribution inside a box with number n as proportional to value of area $S_b^{(n)}$ occupied by coloured matter in this box. A ratio of $S_b^{(n)}$ and S_δ denoted as $D_n = S_b^{(n)}/S_\delta$ can be called a probability density (i.e. a density of distribution). If we average this ratio over the cavity area by calculating the sum $(1/N_\delta)\sum_{n=1}^{N_\delta} D_n$ we get the constant value of ratio of the total area of the coloured matter S_b to S. This value does not change in the course of mixing and is the mean density $\langle D \rangle$,

$$\langle D \rangle = \frac{1}{N_\delta} \sum_{n=1}^{N_\delta} D_n = \frac{S_b}{S}$$

(here and in what follows angle brackets denote an average over the cavity). However, if we consider the square density defined by $D_n^2 = (S_b^{(n)}/S_\delta)^2$ and averaging it over the area of the cavity, we get the inequality:

$$\langle D^2 \rangle = \frac{1}{N_\delta} \sum_{n=1}^{N_\delta} D_n^2 = \frac{1}{S} \sum_{n=1}^{N_\delta} D_n S_b^{(n)} < \frac{S_b}{S}, \tag{15}$$

because $D_n \leqslant 1$ and can not be 1 in the whole cavity (unless the colour matter occupies the whole cavity). Therefore, such a quantity as the statistical square density $\langle D^2 \rangle$ will decrease in time as the dyed material is spread over an increasing number of boxes. In terms of statistical mechanics, D_n is the 'coarse-grained density', which is different from the 'fine-grained density' f_d of the infinitesimal, super-differential elements dS_f, which are always assumed to be small compared to the width of the area of the coloured matter. Moreover, dS_f is always so small that it either is located inside the coloured matter, and f_d equals one, or it is outside the coloured matter, and f_d equals zero. There is a difference in procedure for evaluation of statistical values too. The 'course-grained' averaging means summing over the cavity area (the so-called 'box counting') and dividing the sum by the box number N_δ, but for the 'fine-grained' averaging we must apply an integration procedure, as $\lim dS_f \to 0$.

It was shown by Gibbs [25, Ch. 12] for the special case of mixing of two fluids, which approaches statistical equilibrium, i.e. the perfect mixed state, that the final state of mixing is characterized by a minimum statistical square density $\langle D^2 \rangle$ and this minimum value is $\langle D \rangle^2$. Thus, going to a uniform mixture in time, the mean square density $\langle D^2 \rangle$ will approach its minimum $\langle D \rangle^2$ or, in other words,

$$\left\langle \left(D - \langle D \rangle \right)^2 \right\rangle \tag{16}$$

will go to zero. The rate of decrease of these values is not only time dependent but also depends on the box sizes.

It is also possible to use the analogy of entropy, $-D_n \log D_n$, instead of D_n^2 as a statistical measure. If the dyed material occupies a box completely or is absent, $-D_n \log D_n$ equals to zero. The entropy measure changes only in those boxes, where $0 < D_n < 1$. Moreover, for $0 < D_n < 1$, the value $-\log D_n$ is always positive, so the more boxes the dyed material covers the bigger is $-\sum_{n=1}^{N_\delta} D_n \log D_n$. As a result, for a good mixing process, the entropy of the mixture

$$e = -\langle D \log D \rangle \tag{17}$$

will grow in time to its maximum

$$e_0 = -\langle D \rangle \log \langle D \rangle. \tag{18}$$

The entropy measure is not independent of the square density measure, and both of them are first-order statistics measures (one element of area at a time).

Danckwerts [35] has defined two properties that are useful in evaluating the quality of mixing: the scale of segregation L_C and the intensity of segregation I_C. The scale of segregation is a measure of a size of clumps in a mixture, while the intensity of segregation refers to the variance in composition. For the intensity of segregation he introduced the formula

$$I_C = \frac{\int_S (C - \langle C \rangle)^2 \, dS}{\langle C \rangle (1 - \langle C \rangle) S} = \frac{\langle (C - \langle C \rangle)^2 \rangle}{\langle C \rangle (1 - \langle C \rangle)}, \tag{19}$$

where C is the local concentration, which is in Gibbs's and Welander's definitions equal to the fine-grained density f_d. It is easy to verify that for distributive mixing the fine-grained density $\langle (f_d - \langle f_d \rangle)^2 \rangle = \langle f_d \rangle - \langle f_d \rangle^2$, and in that case I_C always equals one. Consequently, for mixing without diffusion and chemical reaction, the intensity of segregation I_C is not decreasing, but equals the constant, initial value.

Therefore, we suggest a modification of the intensity of segregation, by making the mean square density (16) dimensionless by dividing by $\langle D \rangle (1 - \langle D \rangle)$, namely

$$I = \frac{\langle (D - \langle D \rangle)^2 \rangle}{\langle D \rangle (1 - \langle D \rangle)}. \tag{20}$$

For good mixing $\langle (D - \langle D \rangle)^2 \rangle$ tends to zero, which means that I also tends to zero.

Our definition of I is different from a similar mixing measure I_O used by Ottino [7] who defined this quantity as the square root of the mean square density divided by $\langle D \rangle^2$,

$$I_O^2 = \left\langle \left(D - \langle D \rangle \right)^2 \right\rangle / \langle D \rangle^2. \tag{21}$$

When mixing is studied by analysis of the distribution of N unconnected points and the coarse grain modification I in (20) is used, an additional assumption is needed. This assumption says that to every single point corresponds a small, undeformed by mixing, area S_b/N.

The scale of segregation L_C was defined by Danckwerts [35] by means of the correlation function

$$K_C(\boldsymbol{\eta}) = \left\langle \left(C_1 - \langle C \rangle \right) \left(C_2 - \langle C \rangle \right) \right\rangle \tag{22}$$

which shows how the concentration fluctuations $C - \langle C\rangle$ at points 1 and 2, separated by the vector $\boldsymbol{\eta} = \eta \boldsymbol{e}$, differ from each other. The normalized correlation function is called the correlation coefficient

$$\rho_c(\boldsymbol{\eta}) = \frac{\langle (C_1 - \langle C\rangle)(C_2 - \langle C\rangle)\rangle}{\langle (C - \langle C\rangle)^2\rangle}. \tag{23}$$

It is obvious that $\rho(\mathbf{0}) = 1$. When η exceeds a certain value, the relationship between the concentrations in points may become random and $K_C(\boldsymbol{\eta})$ drops to zero. If a mixture consists of clumps, the value of η at which $K_C(\boldsymbol{\eta})$ (22) is equal to zero (say, $\eta = \xi$) is approximately the average size of the clumps in the direction $\boldsymbol{e}$. More precisely, the average radius of clump in the direction of $\boldsymbol{e}$ is

$$L_C(\boldsymbol{e}) = \int_0^{\xi} \rho_c(\boldsymbol{\eta})\, d\eta. \tag{24}$$

The mixing patterns which we are going to discuss do not consist of a random distribution of clumps, but of layered structures (see *figure 2*). However, the coarse grain representations of these patterns may look like clumps. If we cover area boxes for which the density D_n is larger than $\langle D\rangle$ with black, the boxes where D_n equals to $\langle D\rangle$ with grey, and boxes where $0 \leqslant D_n < \langle D\rangle$ with white, then such representation can be considered as white and black clumps with grey clumps that serve as transitional ones. Moreover, with the coarse-grained correlation function defined as

$$K(\boldsymbol{\eta}) = \left\langle \left(D^{(1)} - \langle D\rangle\right)\left(D^{(2)} - \langle D\rangle\right)\right\rangle \tag{25}$$

(where $D^{(1)}$ and $D^{(2)}$ correspond to coarse-grained density in the boxes 1 and 2 separated by vector $\boldsymbol{\eta}$), the short term regularity, which gives important information about the mixture pattern, can be examined. Short term regularity means that, on average, in two boxes at any distance $\eta < \xi$ the fluctuations $D_n - \langle D\rangle$ have the same sign (i.e. the same colour) and thus $K > 0$. For $\eta = \xi$ the fluctuations become uncorrelated and therefore $K = 0$. Thus, the distance $\eta = \xi$ in the direction $\boldsymbol{e}$ is related to the size of average clump in this direction, and the value

$$L(\boldsymbol{e}) = \int_0^{\xi} \frac{\langle (D^{(1)} - \langle D\rangle)(D^{(2)} - \langle D\rangle)\rangle}{\langle (D - \langle D\rangle)^2\rangle}\, d\eta \tag{26}$$

gives the average radius of the clump. Complementary to intensity of segregation I, the scale of segregation L can be used as a measure of clump sizes of the coarse-grained description of mixing patterns. The dynamics of such scales should reflect the changes of sizes of unmixed regions, where D_n is always larger than $\langle D\rangle$.

In conclusion, in this section we have shown that, with the solution of the velocity field in an annular wedge cavity, the contour line tracking and periodic point search algorithm, and the described mixing measures, we are able to analyse the mixing flow in the cavity in its full details. Also the importance of using the first and the second order mixing measures was elucidated. All of this will be demonstrated in the next section.

3. Results and discussion

The results presented here correspond to the wedge cavity with $\theta_0 = \pi/4$ and $b/a = 2$. To compare the efficiency of different mixing processes we need to measure the supplied energy. We suppose that the periodic protocols as well as the stationary mixing processes have the same angular velocities $2\Theta/T$. Then, a total displacement accomplished by moving walls can serve as a measure of an amount of work done in moving the walls (i.e. the 'input energy'). For the periodic protocols (1), this value is $\Theta(a + b)$ for one period, and

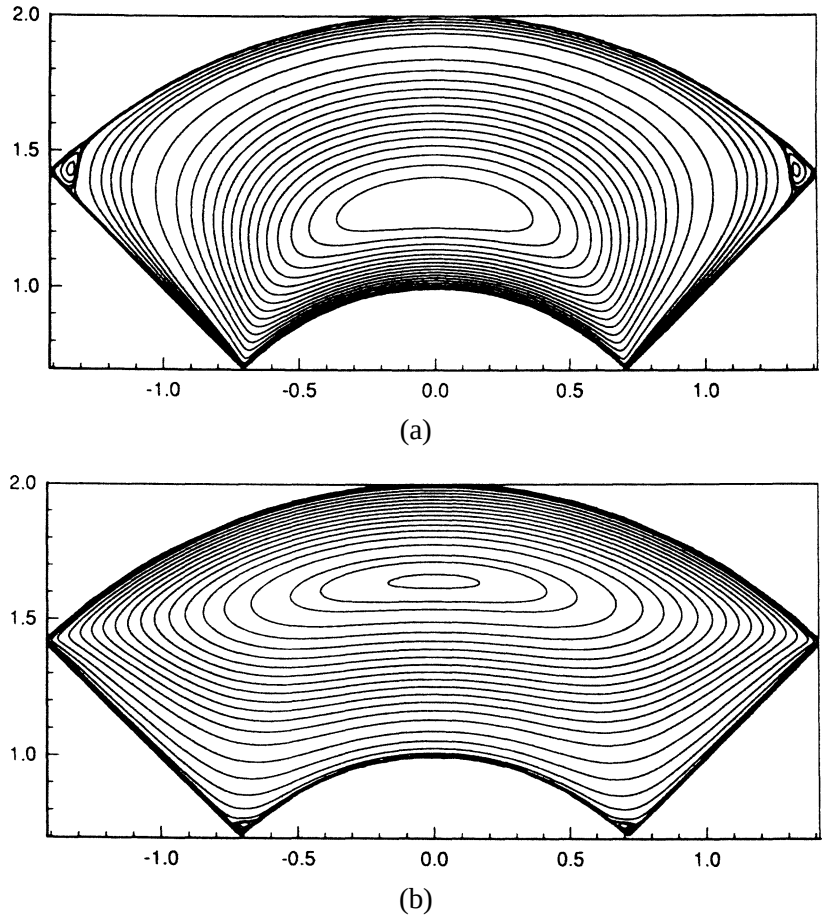

Figure 4. Streamlines patterns, corresponding to the motion of (a) the bottom wall $V_{\text{bot}} = 1,\ V_{\text{top}} = 0$; (b) the top wall $V_{\text{bot}} = 0,\ V_{\text{top}} = 1$.

$\Theta(a+b)N_p$ for N_p periods or, in a dimensionless form, $W = \Theta(a+b)N_p/(\theta_0 a) = 3HN_p$ (where $H = \Theta/\theta_0$). For the stationary mixing, with only the bottom (top) wall moving, $W = \Theta_1/\theta_0$ ($W = 2\Theta_2/\theta_0$), where Θ_1 (Θ_2) is the total angle of rotation during the whole process.

The steady streamline patterns (*figure 4*) for bottom or top wall movement both reveal closed lines around elliptical stagnation points with polar coordinates $(1.31, 0)$ and $(1.64, 0)$, respectively, in the middle of the cavity and the Moffatt eddies near quiet corners. These patterns help us to elucidate the process of steady mixing, presented in *figure 1*.

In the example given in *figure 1(a)*, the blob centre is at the stagnation point corresponding to *figure 4(a)*. In *figure 1(b)* the mixing pattern produced by the motion of only the bottom wall was drawn. The same 'input energy' as during ten periods of the discontinuous protocol with $H = 4$ was used. The light-green coloured area shows where mixing occurs. The mixing pattern created by the top wall motion (again for the same 'input energy') is presented in *figure 1(c)*. This pattern is more uniformly distributed over the cavity area because the mixing domain is larger. This mixing domain is drawn between the boundary streamlines corresponding to trajectories of the uppermost and lowest points of the initial circular contour of the red blob.

Returning to the periodic flows, *figure 5* shows a bifurcation diagram of the dependence on H of the root r^* in (13), for periodic points of period 1. For $H < 4.86$ there exists only one period-1 periodic point. It changes

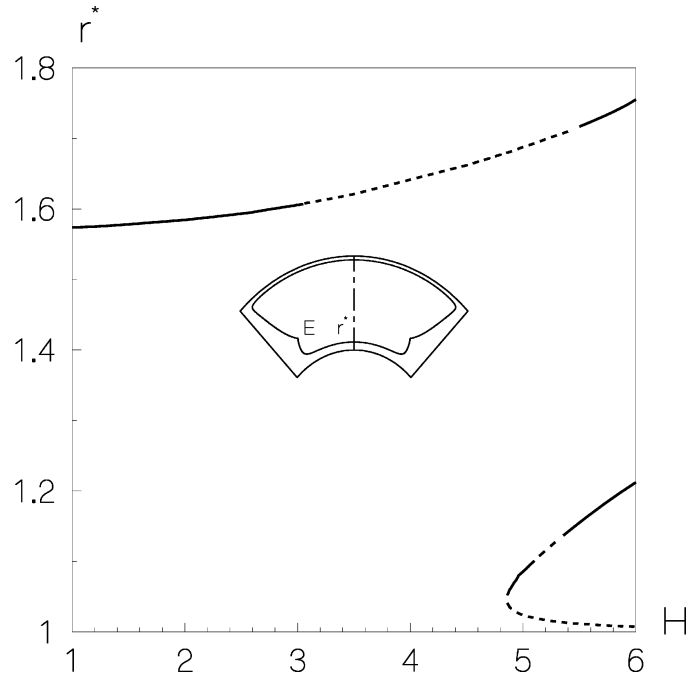

Figure 5. Bifurcation curve showing the dependence of the coordinate r^* on the centreline of the periodic point of period 1 on the protocol parameter H. A typical trajectory of a periodic point E is shown in the small graph in the middle.

its type from elliptic (solid line) to hyperbolic (dashed) while passing a parabolic point at $H = 3.05$. Next, a tangent bifurcation curve appears at $H = 4.86$ and a part of the upper branch at $H = 5.48$ changes type. In what follows we restrict our consideration to the case $H = 4$.

The locations of all periodic points up to period 6 are presented in *figure 6*, apart from those of period 3 and period 5, since they are practically situated at the boundary of the cavity. The periodic points shown are (mainly) of the hyperbolic type which may lead to the conclusion that such a protocol provides good mixing. It is also worth noting that the traditional method of Poincaré mapping with filtering 2, 4 and 6 can hardly reveal even elliptical points of period 2, period 4 and period 6, respectively, because of small sizes of corresponding elliptical islands.

The advantages of the contour line tracking algorithm are seen clearly from *figure 7*, with an initial circular contour of radius $R = 0.2a$ with its centre at the hyperbolic point of period 1. In *figure 7(a)* the initial position of the blob contour line is represented by 25 points. In *figure 7(b)* the interfacial contour line after twelve periods is constructed with about 5×10^4 points. The values for the tracking parameters (see Section 2.2.2) used were $l_{\mathrm{dis}} = 0.03a$ and $l_{\mathrm{cur}} = 0.015a$. It is important to stress that, due to the very strong, nonuniform, exponential stretching, about 40% of the length of the initial contour line (dashed lines in *figures 7(a)* and *7(b)*) corresponds to only 0.2% of the final length. The solid part of the initial contour line is stretched about 10^3 times.

Because of the exponential divergence of neighbouring points, the approach, based upon the representation of the blob contour as an initially uniformly distributed collection of points, can only provide a qualitative picture of mixing and does not conserve its topological properties. *Figure 7(c)* shows the positions of 5×10^4 points initially distributed uniformly along the circle, after twelve periods. If these points are connected (*figure 7(d)*) the picture looks completely different from the one presented in *figure 7(b)*. The length of the contour line in *figure 7(d)* (if one can call this the 'length') is only about 4% smaller than the length of the curve in *figure 7(b)*,

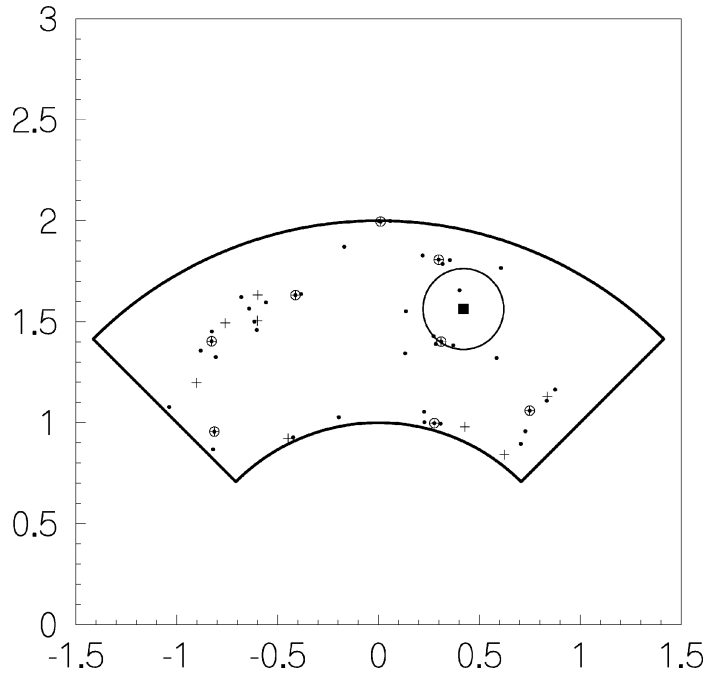

Figure 6. Location of periodic points: the filled square represents the hyperbolic point of period 1; circles indicate the fixed points of period 2; crosses correspond to periodic points of period 4 and bullets to period 6.

but the enclosed area of the dyed material is six times larger. The traditional algorithm needs almost 5×10^7 points in order to obtain the interfacial contour line with the same accuracy in length and area as in *figure 7(b)*.

The accurate Lagrangian description of the contour line provides the opportunity to construct an Eulerian representation of the mixture. *Figure 8(a)* shows the mixed state with the positions of the initially circular blob (yellow area) after six periods (red) and after twelve periods (blue). There are two main components of the coherent structure in the mixed state: one component formed by the thin filaments with their striation decreasing in time, and the other one by the small 'rubbery' region, representing the unmixed part of the blob. What creates this structure? First of all, the invariant unstable manifold corresponding to the hyperbolic point of period 1 which is located in the centre of the original yellow blob (indicated by a black square in the middle in *figure 8(b)*). This manifold, part of which is presented in the *figure 9(a)*, serves as a skeleton which forms the first main coherent structures of the deforming blob. The origin of the 'rubbery' coherent structure can be explained in terms of the existence of the elliptic periodic points of period 2, period 4 and period 6, respectively, which are shown as white boxes in *figure 8(b)*. In the upper part of the yellow circular blob *figure 8(b)*, a small black box indicates the position of the hyperbolic fixed point of period 6, and therefore, the region nearby this point will be destroyed completely in the course of time. The resulting deformation after twelve periods of small circular domains surrounding these higher order periodic points are shown in *figure 9(b)*. The small circular blob surrounding the hyperbolic point transforms after twelve periods into a thin line, while the three circular blobs surrounding the elliptic points only slightly deform.

Next, the application of the statistical measures for the evaluation of the mixed state quality is discussed. Inside every square box deviations from the mean value of a uniform mixture of the square density, intensity and entropy are presented in *figure 10* for the particular blob deformation shown as the blue pattern in *figure 8(a)*.

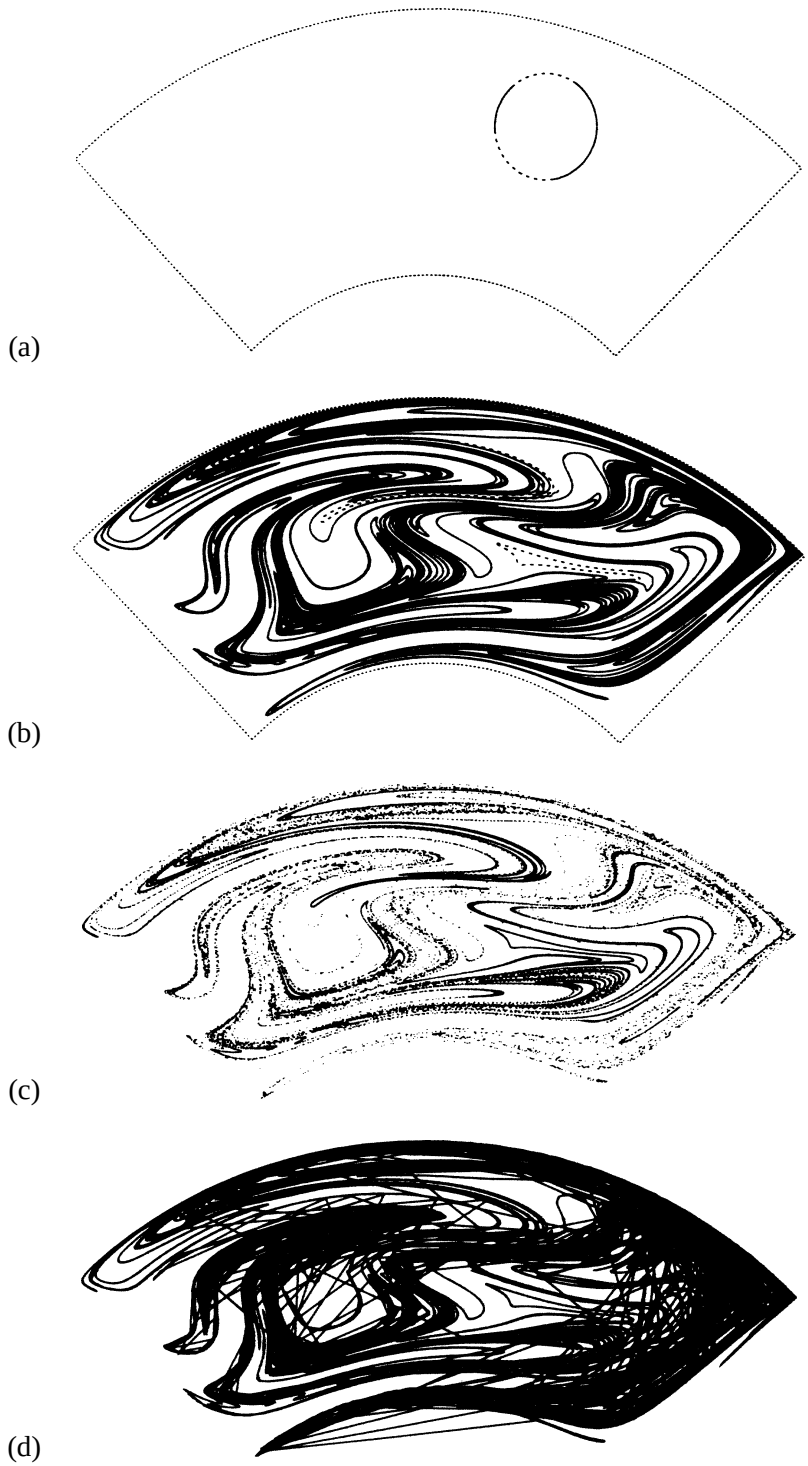

Figure 7. Contour lines: (a) for the initial state; (b) after twelve periods, constructed by the new algorithm; (c) marked by 50,000 points initially uniformly distributed along the circle; (d) after connecting neighbouring points in (c).

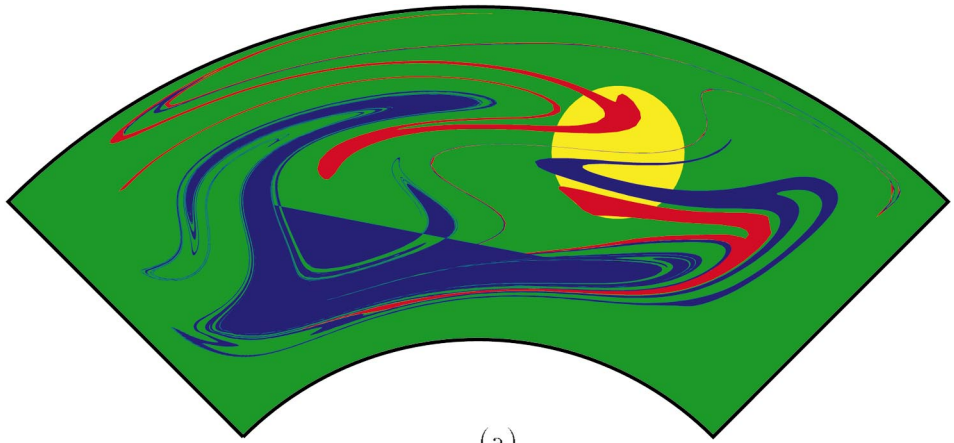

(a)

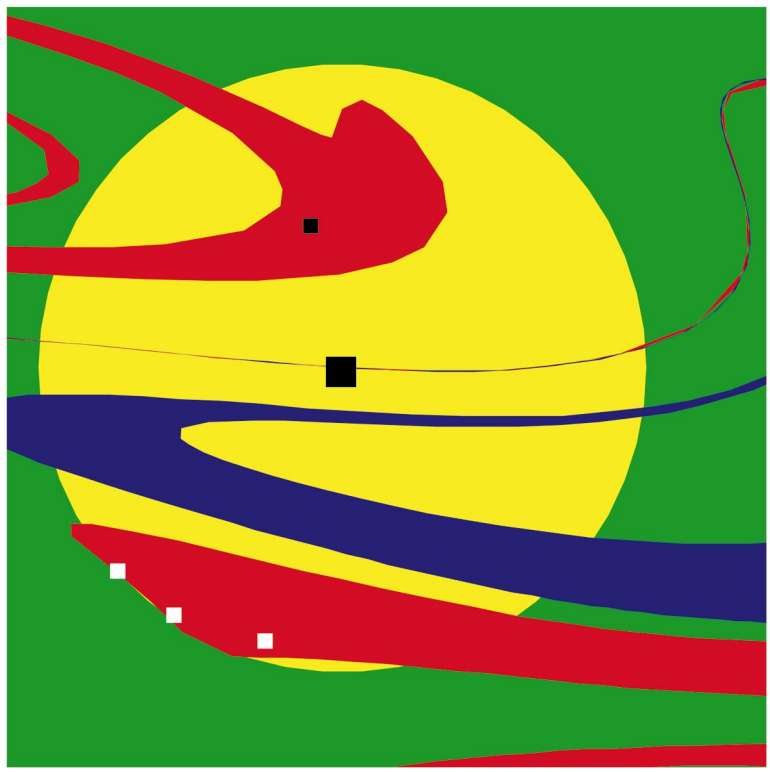

(b)

Figure 8. Mixing patterns: (a) in the whole cavity; (b) in the region of the initial blob position.

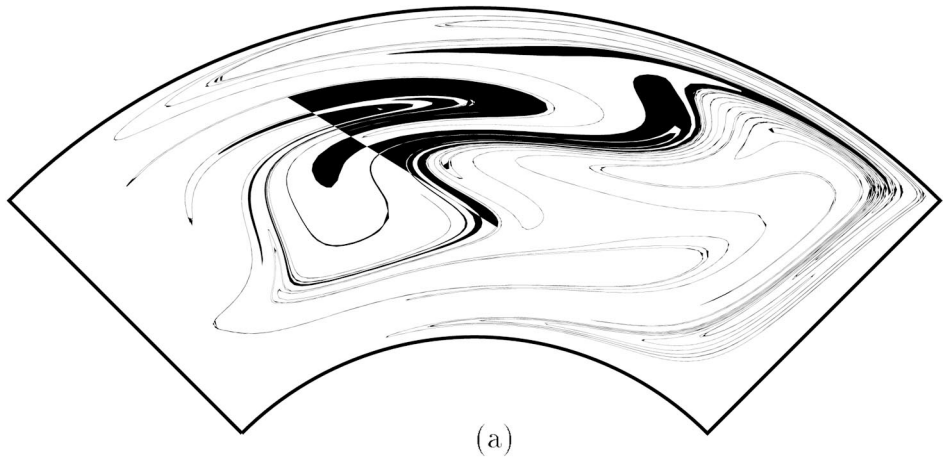

(a)

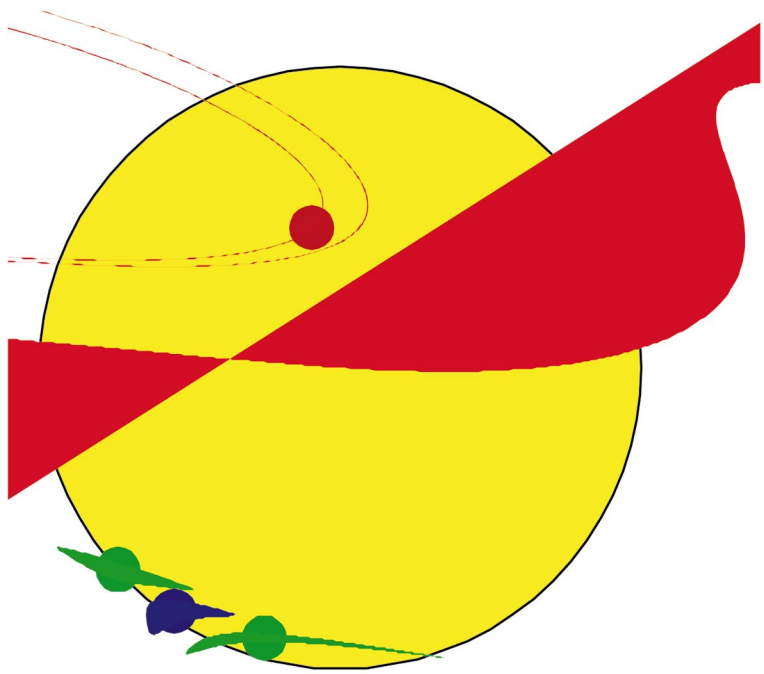

(b)

Figure 9. The elements of coherent structures: (a) part of unstable manifold of the hyperbolic point of period 1 in the centre of the initial blob; (b) deformation patterns of small circular blobs surrounding periodic points of higher order.

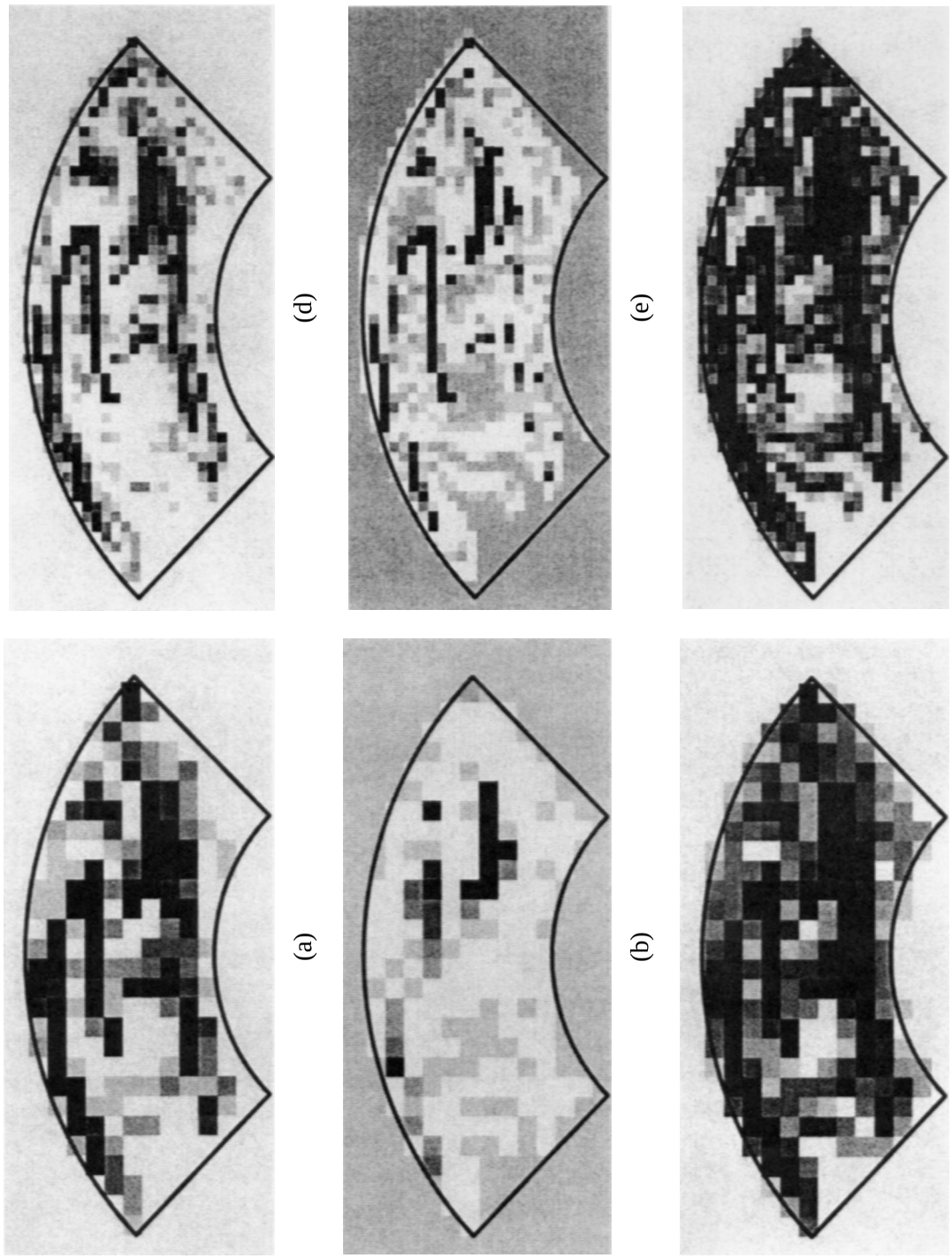

Figure 10. Coarse-grained representations of the mixing pattern shown by the blue colour in *figure 8(a)* for two box sizes $\delta = 0.1a$ and $\delta = 0.05a$ for: (a), (d) square density; (b), (e) intensity of segregation; (c), (f) entropy.

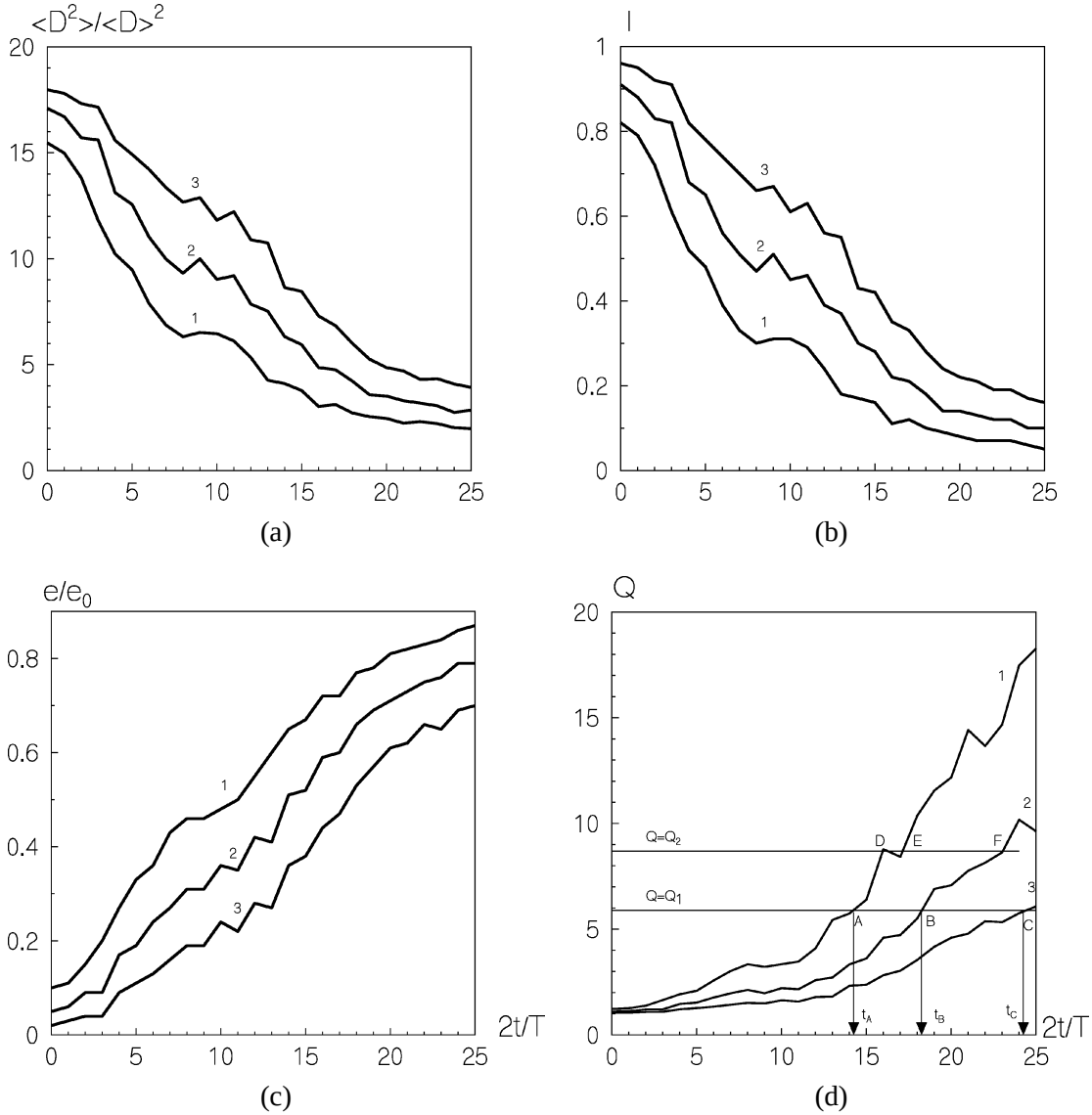

Figure 11. Dynamics of (a) the square density; (b) intensity of segregation; (c) entropy; (d) quality of mixing. The initial blob is shown as the yellow circle in *figure 8(a)*. The three curves in each figure correspond to three different box sizes: 1–$\delta = 0.1a$; 2–$\delta = 0.05a$; 3–$\delta = 0.025a$.

Figure 10 clearly demonstrates that, although the mixing pattern is not clumpy, the coarse grain representations of this pattern look clumpy.

The dynamics in time of the three criteria based on the coarse-grained density D_n are shown in *figure 11* for different box sizes. The mixing protocol and the initial position of the blob are the same as in *figure 8(a)*. The mixing process is characterized by the decrease in square density $\langle D^2\rangle/\langle D\rangle^2$ (*figure 11(a)*) and in the intensity of segregation I (*figure 11(b)*) and by an increase in entropy e/e_0 (*figure 11(c)*). From *figures 11(a)* and *11(b)* it follows that intensity and square density give the same dynamics but in different scales. We prefer to use the intensity because it always lies in the same range $(0, 1)$. Using this criterion it is possible to compare mixing processes for different values of the ratio S_b/S and to compare different mixtures with the same ratio S_b/S.

For instance, it is easy to answer the question of after how much mixing time the intensity of segregation will have some given value for different box sizes (which basically represents the problem of scaling in mixing processes), just by drawing a horizontal line $I = \text{constant}$. If we state that a mixture is uniform (enough) (for a given box size) when I is less then some minimum value $I_{\min}$, we know how long we have to continue the mixing for other box-sizes, i.e. differently sized mixers.

If a number that increases with mixing time is preferred, either the entropy (*figure 11(c)*) or the quality Q, defined as the reciprocal of the intensity I (see *figure 11(d)*) can be used. It is worth noting that for the same box size, the same quality (or intensity) of mixing can be repeatedly reached. Thus, the quality Q of a mixture can decrease for some time during the mixing process after which it starts to increase again.

In *figure 12* results of deformation of a circular yellow blob are presented for different initial locations of the blob. In *figure 12(a)* the blob is centred around an elliptic point of period 2 and covers three hyperbolic points of period 6 and one hyperbolic period 4 point. For this case the stretching is the largest while the distribution of the deformed blob is poorest, with the quality $Q = 4.7$. In *figure 12(b)* the blob is centred around a hyperbolic point of period 2. Stretching is nearly the same as in the previous case, the quality $Q = 5.9$ (since the distribution is better). Finally, *figure 12(c)* shows the deformed blob that was initially centred around a hyperbolic period-1 point. There the stretching is the poorest (only half of the two previous cases) but the distribution looks the best. This is reflected in the quality, $Q = 6.1$. Therefore, values of stretching do not correlate with the values of the quality Q.

The intensity of segregation I was calculated for the case of the largest stretching (*figure 12(a)*) using a set of N points uniformly distributed inside the initial blob area. We already mentioned in Section 1 that there exists no criterion which evaluates the precision of approximation when based on preservation of the number of points N, i.e. preservation of a Lebesgue measure. The calculations with $N = 10^4$ gave, for the mixed pattern like the one in *figure 12(a)*, an error of 35% in the values of intensity of segregation if compared with results from contour tracking. Thus, for mixing with large stretching, calculations with any number of points N sooner or later loose their precision. The approach with contour line tracking does not show this problem because of the preservation of the initial area. Comparison of coarse-grained representations of the intensity of segregation determined by the contour line tracking algorithm and by calculations with uniform distributed points $N = 10^4$ as well as the patterns themselves are shown in *figure 13*. For clarity only a part of the cavity (*figure 12(a)*) is shown: the blob is coloured red while its boundary is indicated with a black contour. It is obvious from these pictures that in the area where the contour line tracking gives a large number of thin filaments (on the right side of the area), which means not much dyed fluid at all, the uniform points approach shows a large amount of points due to large number of the filaments and, consequently, a much higher coarse-grained density (compare *figures 13(b)* and *13(d)*).

Next, let us compare the quality of mixing for different mixing protocols: for stationary motion of the bottom or top walls (*figures 1(b)* and *1(c)*, respectively), for periodic motions with $H = 2$ (*figure 2(a)*) and $H = 4$ (*figure 2(b)*). For all considered cases the total amount of input energy is the same ($W = 148$). Therefore, for the protocol with $H = 2$ the number of periods is twice as much as for the protocol with $H = 4$. Stationary mixing when the blob is initially located at the stagnation (elliptic) point (*figure 1(b)*) and periodic mixing with $H = 2$ and with initial location of the blob at the periodic elliptic point (*figure 2(a)*) provide approximately equal values of the corresponding measures independently of the box size. On the other hand, the stationary mixing with moving the top wall (*figure 1(c)*) provides in the largest size box ($\delta = 0.1a$) the same values of measures as periodic mixing with $H = 4$ with the largest stretching shown in *figure 12(a)*. In the smallest scale $\delta = 0.025a$ this stationary mixing is poorer than any of periodic mixing with $H = 4$ (*figure 12*) but is still better than periodic mixing with $H = 2$ (*figure 2(a)*).

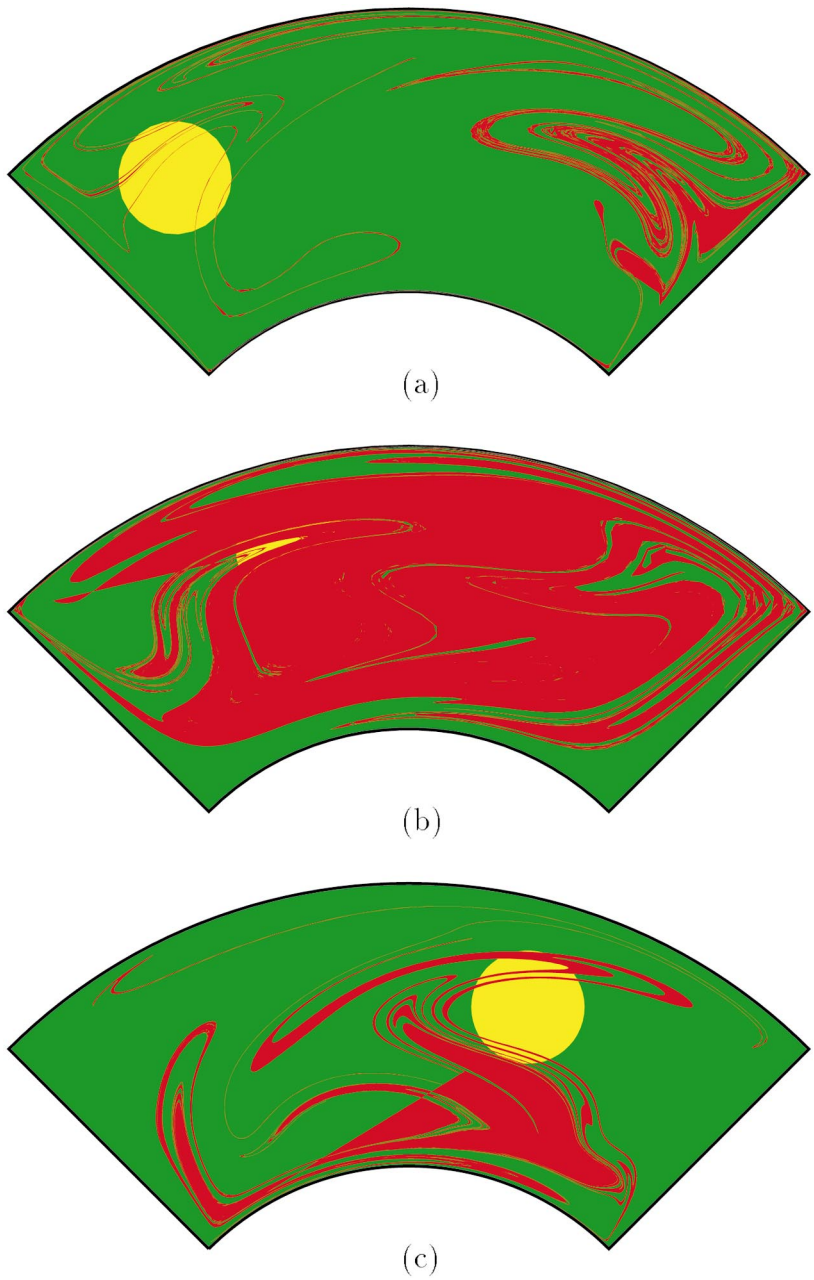

Figure 12. Mixing patterns generated by the same protocol for the different initial locations of the yellow blobs: (a) large stretching; (b) large stretching and relatively good mixing; (c) poor stretching combined with best mixing.

It is interesting to analyse not only the final quality of the mixing processes but also to follow the dynamics of all measures as a function of the input energy W. *Figure 14* presents the comparison of various measures for several mixing protocols. The rate of decrease of $\langle D^2\rangle/\langle D\rangle^2$ and I and increase of e/e_0 and Q for stationary mixing with the top or bottom moving wall (curves 2 or 3, respectively) is moderate. The slowest mixing (curves 4) corresponds, however, to the periodic process with $H = 2$ and the initial blob centred at the elliptic

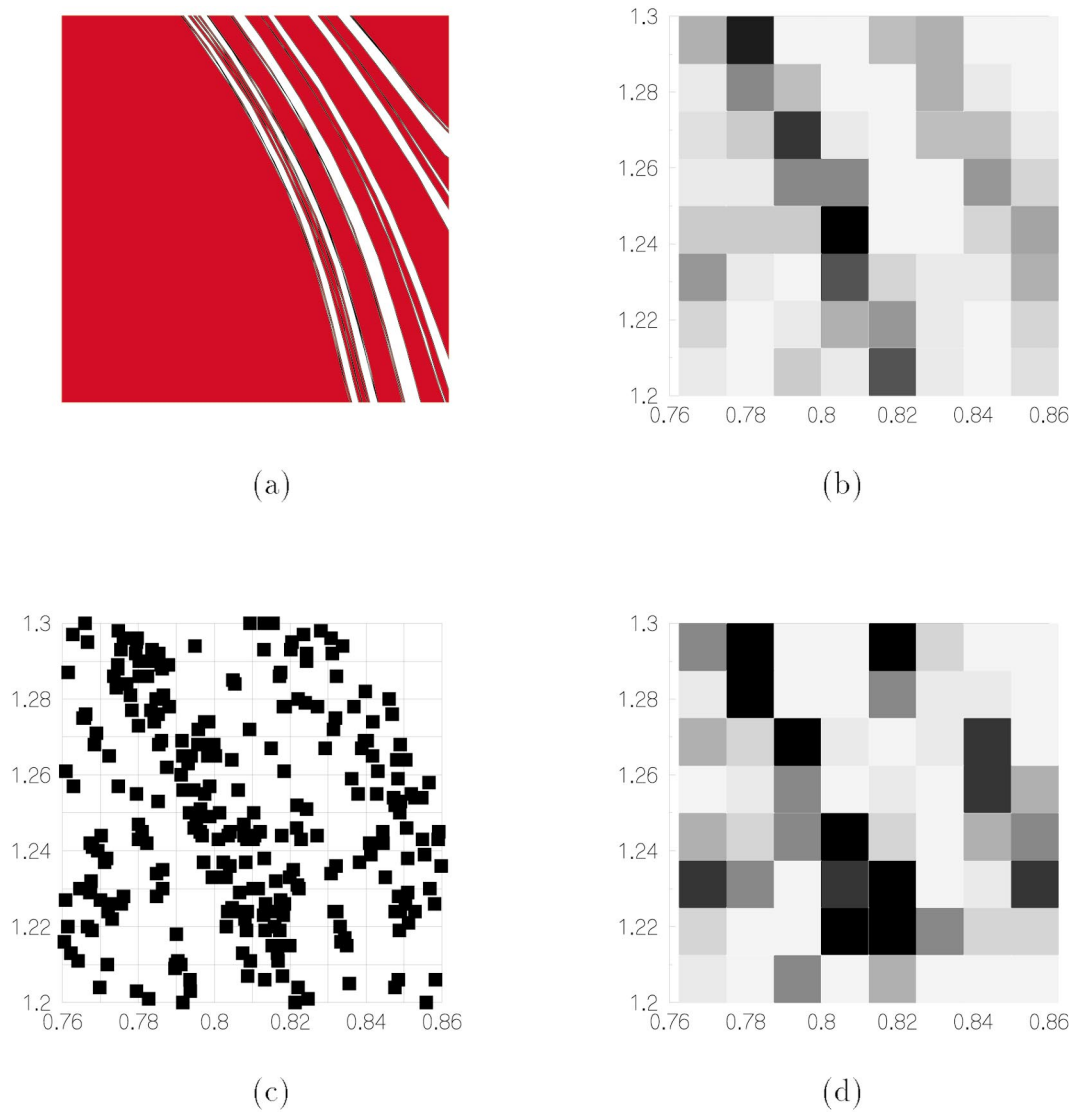

Figure 13. Mixing pattern (a) and intensity of segregation representation (b) using contour line tracking, and $N = 10^4$ point approximation for the pattern (c) and intensity (d).

point of period 1 (see mixing pattern in *figure 2(a)*). The chaotic mixing of the blob located at the hyperbolic period-1 point with $H = 4$ (curves 1) is the best. The data presented in *figure 14* show that final values of measures for regular periodic mixing (curves 4) and for stationary mixing (curves 3) are reached already at a half of the input energy for the chaotic (curves 1) and other stationary mixing (curves 2). This means that periodic mixing is not always better than the stationary one—the specific location of the initial blob (nearby hyperbolic points) is of crucial importance. Therefore, optimization of mixing for a given energy input must be based not only upon the comparisons of the protocols themselves but upon consideration of the initial positions of the blobs. Moreover, among various hyperbolic periodic points, the point for which the unstable manifold covers more uniformly the whole cavity should be preferred as a blob's centre (compare *figures 12(a)* and *12(c)*). Besides, the initial splitting of the blob into several smaller blobs (if possible) can provide the best

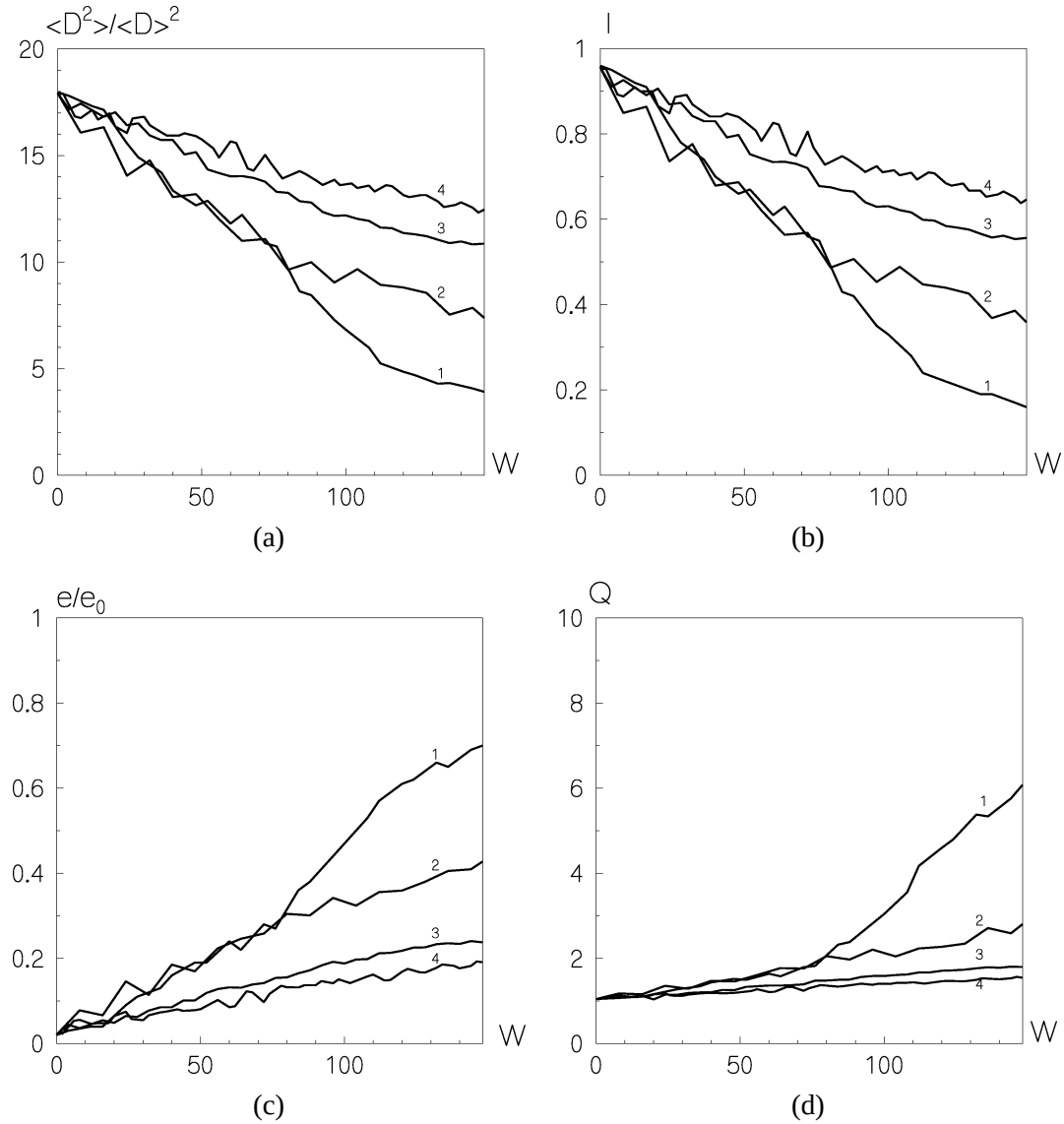

Figure 14. Dynamics of (a) square density; (b) intensity of segregation; (c) entropy; (d) quality of mixing in the smallest box size $\delta = 0.025a$. Curves 1 (curves 4) correspond to periodic mixing with $H = 4$ ($H = 2$) and the blob centred at the hyperbolic (elliptic) point. Curves 2 (curves 3) represent measures for stationary mixing with the top (bottom) moving wall.

mixing under the same protocol and energy input (see *figure 2(c)*). It is worth noting that all four measures give the same qualitative conclusions. Therefore, any of these criterion can be used for estimating the mixing quality. For dispersive laminar mixing the intensity I is generally accepted (see Brodkey [5]) and it is logical to use Q to judge the related energy, as both are increasing quantities.

An important issue is connected with the time reversibility of all measures. There are two questions in this issue. One concerns the reversibility of individual points, representing the contour line after some time T_R, to their initial positions at time $2T_R$. The second question is connected with the conservation of the blob area and, therefore, reversibility of all measures. Calculations with 30000 points 'uniformly' distributed along the initial contour line presented in *figure 7(a)* have shown the accurate reversibility after ten periods. In spite of

the accurate calculations of the individual point positions already after the two first periods, the blob area was not conserved, the relative error after the nine periods was, for example, 70% (meaning that 70% of the original blob area has been 'lost'). The calculations based on our algorithm with 'nonuniform' distribution of points conserved the blob area for twelve periods of forward and twelve periods of backward motions (a check on area conservation showed that even after 12 periods of forward motion less than 1% of the dyed material was lost, see discussion of *figure 7*). In this case the computations of all coarse grained measures based on the value of the blob area are reliable. Nevertheless, for such computations not all points come back to their initial positions. After the reverse process some of the points are located along pieces of the unstable manifold for the backward motion (which coincides with the stable manifold for the forward motion). The contribution of these spurious lines to the blob area equals zero. Thus, we can conclude that computation of the measures shows a complete reversibility in spite of irreversibility of some individual points.

Now, we address the second-order measures of mixing quality, since these measures indicate the relative size of unmixed 'rubbery' domains. Criteria like those could be, practically, more relevant than those of the first-order statistics dealt with so far. In *figure 15(a)* the dynamics of the scales of segregation in two directions $\boldsymbol{x}$ and $\boldsymbol{y}$ are shown for the same mixing process as was used for calculations of the first-order statistics (*figure 11*) for the same three box sizes. Initially, the scales in the $\boldsymbol{x}$-direction (solid lines) and $\boldsymbol{y}$-direction (dashed lines) are almost equal and give the approximate value of the radius of the initial blob ($R = 0.2a$). For the box counting with $\delta = 0.1a$ (curve 1 in *figure 15(a)*) the error of the value of R is about 9%, in counting with $\delta = 0.05a$ (curve 2 in *figure 15(a)*) as well as in counting with $\delta = 0.025a$ (curve 3 in *figure 15(a)*) it is slightly larger. In the course of time, due to the anisotropy of the patterns (see *figures 2(b), 7(b), 8(a), 12(c)*), the dimensionless scale of segregation in $\boldsymbol{x}$-direction $L_x = L(\boldsymbol{x})/a$ and in the $\boldsymbol{y}$-direction $L_y = L(\boldsymbol{y})/a$ diverges. Nevertheless, both have a tendency to decrease, but not uniformly in time. In *figure 15(b)* the dependence of the averaged scale $L = (L_x + L_y)/2$ on time is presented for the three box sizes. After the two first periods of mixing, the curves can be approximated by exponential functions of the form $c_i + c_0 e^{-ct/T}$. These functions are drawn in *figure 15(b)* as dashed lines 4, 5 and 6, respectively. Using those approximations we can roughly estimate after how many periods the averaged scale of segregation L will be smaller than some given value. For example, for

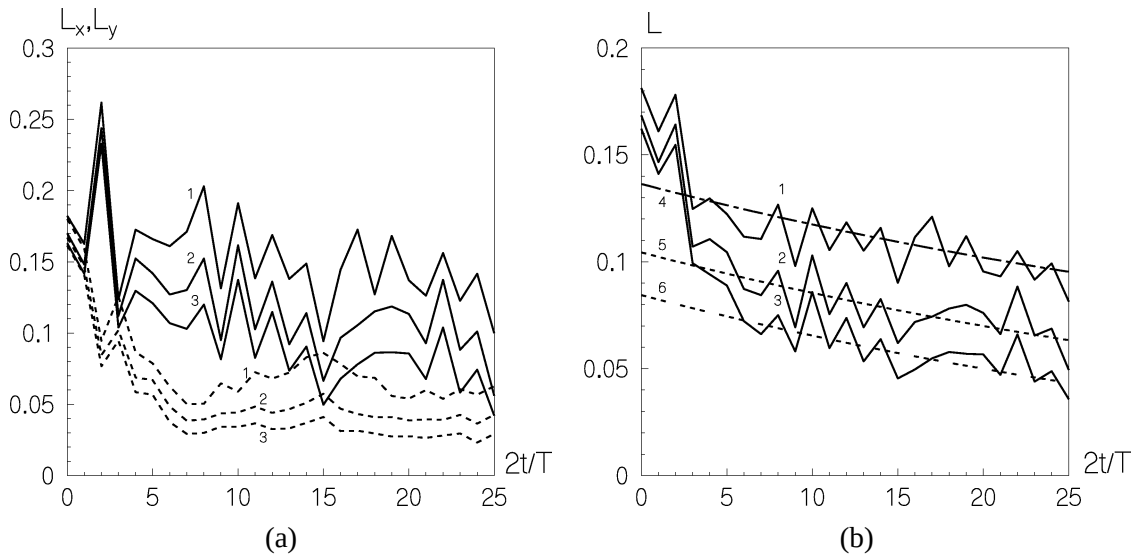

Figure 15. Dynamics of the scales of segregation (a) L_x and L_y; (b) the averaged scale L (solid) with the approximation $c_i + c_0 \exp(-ct/T)$, $c_0 = 0.1$ and $c = 0.04$. Dashed curves: 4 ($c_i = 0.03$); 5 ($c_i = 0$); 6 ($c_i = -0.02$).

the counting with $\delta = 0.05a$, L becomes less than $\delta/2$ (the unmixed 'rubbery' domain is smaller than the area of the box) after approximately 35 periods.

Thus, the existence and change of the unmixed 'rubbery' domains in the mixture pattern can be determined from the behaviour of the scales of segregation. For one unmixed zone, like the initial situation with one circular blob, scales (26) directly give the size of the blob. For the well-mixed patterns of high quality, the non-zero values indicate the existence of unmixed domains that decline very slowly (or even stabilize, when the zone does not diminish in size at all) despite continuing mixing.

The dynamics in time of the first-order statistical measurements (square density, intensity of segregation, entropy and quality) are different from the dynamics of the scale of segregation. The first ones reflect the distribution of filaments over the mixing domain, while the latter show the behaviour of the unmixed domains of the coherent structure. They also change in opposite ways when changing the box size: the smaller the box size, the worse is the mixing according to the first measures and the better according to the scale measures, which decrease with decreasing of the sizes. Therefore, it is necessary to use both measures to judge how well or badly materials are mixed.

4. Conclusions

We briefly summarize the main results of this study.

1. The analytical method of superposition for defining the velocity field and the numerical algorithm for two-dimensional contour line tracking that conserves topological properties of any blob furnish a solid basis for obtaining distributive mixing patterns for the Stokes flow in an annular wedge cavity.
2. An effective algorithm of one-dimensional searching of periodic points in this type of flow is described. Coherent structures related to hyperbolic and elliptic periodic points in distributive mixing patterns are classified. The structure of unstable manifolds of hyperbolic periodic points plays a crucial role in distributive mixing.
3. Based upon the area-preservation property of a closed fluid contour the modified quantities of intensity of segregation and scale of segregation for evaluation of the quality of distributive mixing are developed.
4. At least two independent measures are necessary for estimation of mixing quality, one answering the question how well the deformed blob is distributed over the whole cavity area (e.g. the intensity of segregation or, analogously: square density, entropy or quality) and the second—how large are the non-mixed areas ('rubbery' islands) relative to predeformed characteristics (e.g. the scale of segregation).
5. All quantitative measures: square density, entropy, quality and intensity and scale of segregation—reveal nonmonotonic behaviour in time while approaching their limits for uniform mixtures.
6. A large amount of (exponential) stretching does not always correspond to the best quality of the mixture. In particular, a steady mixing protocol with low stretching of contour lines can sometimes even create a better mixture than a periodic protocol with the same amount of supplied 'energy' if a blob is initially located around some specific hyperbolic point of a higher order.
7. To optimise mixing for the given periodic protocol supposes proper choosing of the initial location of the blob in the cavity. Such a choice should be performed by knowing positions and types of periodic points, structure of unstable manifolds corresponding to hyperbolic periodic points (the first main element of mixing coherent structures) and size of 'rubbery' islands corresponding to elliptic periodic points (the second element of mixing coherent structures).

We suggest that the exposition of the underlying assumptions and general methods for the prototype flow in the annular wedge cavity is sufficient to give an insight into what can happen in more complicated cases. This is the topic of the current investigations in our laboratory.

Appendix: Expressions for sums

The equalities

$$\frac{\cosh\beta\,\theta}{\cosh\beta\,\theta_0} = \sum_{\nu=1,3,\ldots}^{\infty} \left[e^{-\beta\,(\nu\theta_0-\theta)} + e^{-\beta\,(\nu\theta_0+\theta)}\right],$$

$$\frac{\sinh\beta\,\theta}{\sinh\beta\,\theta_0} = \sum_{\nu=1,3,\ldots}^{\infty} \left[e^{-\beta\,(\nu\theta_0-\theta)} - e^{-\beta\,(\nu\theta_0+\theta)}\right]$$

permit us to transform functions $P_+(\rho,\theta)$ and $P_-(\rho,\theta)$ in (11) into the fast convergent on ν series

$$\begin{cases} P_+(\rho,\theta) = \displaystyle\sum_{\nu=1,3,\ldots}^{\infty} \left[\sin(\theta_0-\theta)\,S_+(\rho,\nu\theta_0-\theta) + \sin(\theta_0+\theta)\,S_+(\rho,\nu\theta_0+\theta)\right], \\ P_-(\rho,\theta) = \displaystyle\sum_{\nu=1,3,\ldots}^{\infty} \left[\sin(\theta_0-\theta)\,S_-(\rho,\nu\theta_0-\theta) + \sin(\theta_0+\theta)\,S_-(\rho,\nu\theta_0+\theta)\right], \end{cases} \tag{27}$$

where

$$\begin{cases} S_+(\rho,\eta) = \displaystyle\sum_{n=1}^{\infty} \frac{1}{\beta_n} e^{-\beta_n\eta}\sin\beta_n\rho = \frac{l_0}{\pi}\arctan\left[\frac{\sin(\pi\rho/l_0)}{e^{\pi\eta/l_0}-\cos(\pi\rho/l_0)}\right], \\ S_-(\rho,\eta) = \displaystyle\sum_{n=1}^{\infty} \frac{(-1)^n}{\beta_n} e^{-\beta_n\eta}\sin\beta_n\rho = -\frac{l_0}{\pi}\arctan\left[\frac{\sin(\pi\rho/l_0)}{e^{\pi\eta/l_0}+\cos(\pi\rho/l_0)}\right]. \end{cases} \tag{28}$$

In spite of their complicated expressions, the terms in series (27) and their first partial derivatives decay exponentially with ν. Only a few first terms (usually, $\nu \leqslant 5$) with obvious limits for the term with $\nu = 1$ at the boundary are enough to provide an excellent accuracy of calculations of the velocity field in the whole cavity.

Acknowledgements

We gratefully acknowledge Mr Chritiene Aarts for providing the code for construction of the colour figures. This research is supported by the Dutch Technology Foundation (STW) under grant number STW EWT 44.3453.

(Website: http://www.stw.nl/projecten/E/ewt44.3453.html.)

References

[1] Irving H.F., Saxton R.L., Mixing of high viscosity materials, in: Uhl V.W., Gray J.B. (Eds), Mixing, Theory and Practice, Vol. 2, Academic, London, 1967, pp. 169–224.

[2] Edwards M.F., Laminar flow and distributive mixing, in: Hardy N., Edwards M.F., Nienow A.W. (Eds), Mixing in the Process Industries, Butterworth, London, 1985, pp. 202–225.

[3] Ottino J.M., Mixing, chaotic advection, and turbulence, Annu. Rev. Fluid Mech. 22 (1990) 207–253.
[4] Ottino J.M., Jana S.C., Chakravarthy V.S., From Reynolds's stretching and folding to mixing studies using horseshoe maps, Phys. Fluids 6 (1994) 685–699.
[5] Brodkey R.S., The Phenomena of Fluid Motions, Addison-Wesley, London, 1967.
[6] Middleman S., Fundamentals of Polymer Processing, McGraw-Hill, New York, 1977.
[7] Ottino J.M., The Kinematics of Mixing: Stretching, Chaos and Transport, Cambridge University Press, Cambridge, 1989.
[8] Baird D.G., Collias D.I., Polymer Processing: Principles and Design, Butterworth, London, 1995.
[9] Hopf E., On causality, statistics and probability, J. Math. Phys. 13 (1934) 51–102.
[10] Aref H., Stochastic particle motion in laminar flows, Phys. Fluids A-Fluid 3 (1991) 1009–1016.
[11] Arnold V.I., Avez A., Ergodic Problems of Statistical Mechanics, Benjamin, New York, 1968.
[12] Maxwell J.C., Essay for the Eranus Club on science and free will. Does the progress of physical science tend to give any advantage to the opinion of necessity (or determinism) over that of the contingency of events and the freedom of the will?, in: Harman P.M. (Ed.), The Scientific Letters and Papers of James Clerk Maxwell, Vol. 2, Cambridge University Press, Cambridge, 1995, pp. 814–823.
[13] Borel E., La mécanique statistique et l'irréverssibilité, J. Phys. 3 (1913) 189–196.
[14] Krylov N., Relaxation processes in statistical systems, Nature 153 (1944) 709–710.
[15] Krylov N.S., The process of relaxation of statistical systems and the criterion of mechanical instability, in: Works on the Foundations of Statistical Physics by Nikolai Sergeevich Krylov, Princeton University Press, Princeton, 1979, pp. 193–238.
[16] Lighthill J., The recently recognized failure of predictability in Newtonian mechanics, P. Roy. Soc. Lond. A Mat. 407 (1986) 35–50.
[17] Artuso R., Anomalous diffusion in classical dynamical systems, Phys. Rep. 290 (1997) 37–47.
[18] Spencer R.S., Wiley R.M., The mixing of very viscous liquids, J. Colloid Interf. Sci. 6 (1951) 133–145.
[19] Maxwell J.C., On the displacement in a case of fluid motion, P. Lond. Math. Soc. 3 (1870) 82–87.
[20] Riecke E., Beiträge zur Hydrodynamik, Ann. Phys. Chem. (Ser. 2) 36 (1889) 322–334.
[21] Morton W.B., On the displacements of the particles and their paths in some cases of two-dimensional motion of a frictionless liquid, P. Roy. Soc. Lond. A Mat. 89 (1913) 106–124.
[22] Aref H., Stirring by chaotic advection, J. Fluid Mech. 143 (1984) 1–24.
[23] Chaiken J., Chevray R., Tabor M., Tan Q.M., Experimental study of Lagrangian turbulence in a Stokes flow, P. Roy. Soc. Lond. A Mat. 408 (1986) 165–174.
[24] Aref H., El Naschie M.S. (Eds), Chaos Applied to Fluid Mixing, Pergamon, London, 1994.
[25] Gibbs J.W., Elementary Principles in Statistical Mechanics, Scribner, New York, 1902.
[26] Ehrenfest P., Afanasieva-Ehrenfest T., Begriffliche Grundlagen der statistischen Auffassung in der Mechanik, in: Klein F., Müller C. (Eds), Encyklopädie der mathematischen Wissenschaften, Vol. 4, IV, Art. 32, Teubner, Leipzig, 1907–1914, pp. 3–90. Reprinted in: Ehrenfest P., Collected Scientific Papers, North-Holland, 1959, pp. 213–300. English translation: The Conceptual Foundations of the Statistical Approach in Mechanics, Cornell University Press, 1959.
[27] Jana S.C., Metcalfe G., Ottino J.M., Experimental and computational studies of mixing in complex Stokes flows: the vortex mixing flow and multicellular cavity flows, J. Fluid Mech. 269 (1994) 199–246.
[28] Liu M., Muzzio F.J., Peskin R.L., Quantification of mixing in apereodic chaotic flows, Chaos Soliton. Fract. 4 (1994) 869–893.
[29] Meleshko V.V., Peters G.W.M., Periodic points for two-dimensional Stokes flows in a rectangular cavity, Phys. Lett. A 216 (1996) 87–96.
[30] de Vogelaere R., On the structure of symmetric periodic solutions of conservative systems, with applications, in: Lefschetz S. (Ed.), Contribution to the Theory of Nonlinear Oscillations, Vol. 4, Princeton University Press, Princeton, 1958, pp. 53–84.
[31] Franjione J.G., Leong C.-W., Ottino J.M., Symmetries within chaos: a route to effective mixing, Phys. Fluids A-Fluid 1 (1989) 1772–1783.
[32] Franjione J.G., Ottino J.M., Symmetry concepts for geometric analysis of mixing flows, Philos. T. Roy. Soc. A 338 (1992) 301–323.
[33] Meleshko V.V., Krasnopolskaya T.S., Peters G.W.M., Meijer H.E.H., Coherent structures and scales of Lagrangian turbulence, in: Gavrilakis S., Machiels L., Monkewitz P.A. (Eds), Advances in Turbulence VI, Kluwer, Dordrecht, 1996, pp. 601–604.
[34] Welander P., Studies of the general development of motion in a two-dimensional ideal fluid, Tellus 7 (1955) 141–156.
[35] Danckwerts P.V., The definition and measurement of some characteristics of mixtures, Appl. Sci. Res. A 3 (1952) 279–296.
[36] Ben-Naim A., Is mixing a thermodynamic process?, Am. J. Phys. 58 (1987) 725–733.
[37] Tucker C.L., Principles of mixing measurements, in: Rauwendaal C. (Ed.), Mixing in Polymer Processing, Dekker, Basel, 1991, pp. 101–127.
[38] Press W.H., Teukolsky S.A., Vetterling W.T., Flannery B.P., Numerical Recipes in FORTRAN (2nd edn), Cambridge University Press, Cambridge, 1992.
[39] Krasnopolskaya T.S., Meleshko V.V., Peters G.W.M., Meijer H.E.H., Steady Stokes flow in an annular cavity, Q. J. Mech. Appl. Math. 49 (1996) 593–619.
[40] Goodier J.N., An analogy between the slow motion of a viscous fluid in two dimensions, and systems of plane stress, Philos. Mag. (Ser. 7) 17 (1934) 554–576.
[41] Taylor G.I., On scraping viscous fluid from a plane surface, in: Schäfer M. (Ed.), Miszellangen der Angewandten Mechanik (Festschrift Walter Tollmien), Akademie, Berlin, 1962, pp. 313–315.
[42] Batchelor G.K., An Introduction to Fluid Dynamics, Cambridge University Press, Cambridge, 1967.
[43] Moffatt H.K., Viscous and resistive eddies near a sharp corner, J. Fluid Mech. 18 (1964) 1–18.
[44] Hairer E., Nørset S.P., Wanner G., Solving Ordinary Differential Equations. I. Nonstiff Problems, Springer, Berlin, 1987.